

# We are IntechOpen, the world's leading publisher of Open Access books Built by scientists, for scientists

4,800

Open access books available

122,000

International authors and editors

135M

Downloads

Our authors are among the

154

Countries delivered to

TOP 1%

most cited scientists

12.2%

Contributors from top 500 universities



WEB OF SCIENCE™

Selection of our books indexed in the Book Citation Index  
in Web of Science™ Core Collection (BKCI)

Interested in publishing with us?  
Contact [book.department@intechopen.com](mailto:book.department@intechopen.com)

Numbers displayed above are based on latest data collected.  
For more information visit [www.intechopen.com](http://www.intechopen.com)



# SiC, from Amorphous to Nanosized Materials, the Exemple of SiC Fibres Issued of Polymer Precursors

Philippe Colomban

LADIR, CNRS – Université Pierre-et-Marie-Curie  
France

## 1. Introduction

Silicon carbide materials are interesting because of their high thermal stability, high thermal conductivity, extreme hardness and good electrical properties. Some of these properties are directly related to the SiC structure that alternates the Si and C atom layers. SiC have applications as single crystal wafer (wide-gap semiconductor for high power device), as air, spacecraft and nuclear plant thermostructural composites because it is possible to prepare the materials in various forms (fibre, matrix and composite) from organic liquid or vapour precursors. Thus it is possible to adjust the crystallinity, from the amorphous to the crystalline state, including intermediate nanocrystalline state. The later state guaranties the optimal mechanical properties. Non-destructive Raman microspectrometry intrinsically probes the matter at the subnanoscale and offers a "bottom-up" approach that is especially efficient for the analysis of ill-crystallised and nanostructured materials. The great advantage of Raman spectroscopy is first to make possible the recording of series of spectrum by automatic mapping. However, because the Raman intensity depends on the polarisability tensor derivative, the scattered intensity – and the sensitivity – varies order of magnitude with the nature of the chemical bond. Comparison with transmission electron microscopy (TEM) is in general required to discriminate if the phonon coherence length is determined by the domain or the grain size. Both techniques are efficient to identify the different polytypes as well as the nature and degree of the disorder.

## 2. About the chemistry

The properties of the materials are determined by their chemical bonds and the arrangement of the latter. The uniqueness of silicon carbide properties arises from the nature of the bond. Si-C bond as Si-O and Si-N ones are among the strongest chemical bonds in the matter (Bond dissociation energy > 350 KJ/mole). Consequently, this gives a very good chemical and thermal stability as well very high melting temperature, high mechanical properties and hardness. Silicon atoms form with C, N and O atoms the same tetrahedral coordination that allows very intimate mixture (oxycarbides, oxynitrides, etc.). Furthermore, a hydrogen atom can establish a bond with these oxygen, nitrogen and carbon atoms. This offers a large versatility of preparation routes, including polymerisation process. Consequently, because

silicon and carbon atoms form easily X-C and X-H bonds, a large variety of liquid or gaseous hybrid/organic precursors are available (Mc Diarmid, 1961; Fritz et al., 1965; Corriu & Lanneau, 1970; Lucke et al., 1997) and the control of their reactivity, viscosity/diffusivity dilution, etc. gives rise to a variety of preparation routes leading to monoliths, films, fibres, composites, crystal..., from the amorphous state to the single crystal, including nanomaterials (Gough & Kern, 1967; Parlier & Colomban, 1996; Naslain, 2004).

The mix of atomic orbital led to an intermediate electric behaviour between that of carbon (a semi-metal) and silica (an insulator), the electronic gap is intermediate (2-3 eV) and the material is a semiconductor. Since the diffusion coefficient of oxygen atom in silica is very low (due to the very covalent character of the Si-O bond), the oxidation is blocked in a very large temperature range (except in water-rich atmosphere when volatile species are formed) that gives a good stability to Si(X)<sub>n</sub> compounds in air. The latter properties are searched for thermomechanical applications: the nanosized state combines the advantage of amorphous (homogeneity, lack of interface/phases) and crystalline (high density of bonds per volume unit) phases. Very high thermal conductivity contributes well to the unique properties of silicon carbide. Since nothing is perfect, the building of the SiC with a single type of bond makes that orientation disorder is possible and gives rise to two types of Si-C bilayer stacking. Their combination leads to series of structures: the polytypes and it is difficult to prepare materials without coexistence of the different phases. This behaviour is observed for all structures which are built up by corner-sharing tetrahedron. They can be regarded as consisting of stacked bi-layers.

The availability of volatile/liquid silanes led to the preparation of SiC materials in various forms (McDiarmid, 1961; Fritz et al., 1965; Gough & Kern, 1967; Learn & Khan, 1970; Corriu & Lanneau, 1970; Kumar & Litt, 1988; Schmidt et al., 1991): films/coatings (Rynders et al., 1991), fibres (a SiC coating is deposited on a carbon fibre core (Hurwitz et al., 1991; Tanaka et al., 1995; idem, 1996; Popovska et al., 1997), monoliths and fibre-reinforced composites (Yajima et al., 1980; Tanaka & Kurachi, 1988; Bouillon et al., 1991 a & b; Monthieux et al., 1990; idem, 1991; Delplancke et al., 1991; Lee & Yano, 2004). The growth rate was slow and for the preparation of thick monoliths or composites weeks are required with sometimes an intermediate machining of the parts in order to avoid the closure of the porosity that occurs at the sample surface, avoiding the completion of the core densification. This technology was used to prepare important parts of civil and military launch vehicles, missiles as well as aircraft engines (Parlier & Colomban, 1996; Mouchon & Colomban, 1996; Naslain, 2004) and extended to the preparation of other Si-based materials such as nitrides (Durham et al., 1991).

In the 80s Japanese groups developed liquids with appropriate viscosity (polycarbosilanes: PCS) as precursors for SiC fibre (Okamura et al., 1985). The difficulty concerned the production of a form of polycarbosilane which would have the "good" viscosity to be spun and then converted in small-diameter ceramic filaments. The small diameter (~10 µm) is required to permit the bending of the fibre during the weaving process and hence to prepare a variety of textile fabrics: satin, taffeta, etc. (Mouchon & Colomban, 1995; idem, 1996). It was found that very high molecular weight was not necessarily best and polymers with molecular weights of around 1500 were used for commercial production. Then the progress allowed preparing more complex compositions (Si/TiC, etc. (Stewart et al., 1991; Hasegawa et al., 1991; Burns et al., 1992; Hurwitz et al. 1993)) under more complex states (Tanaka et al., 1988; Langguth, 1995). The viscosity was adapted for an easy infiltration of the precursor

in the porous performs (Greil, 1995; Parlier & Colomban, 1996; Lucke et al., 1997; Greil, 2000) and the technology was extended to multicomponent oxide precursors with the development of sol-gel routes (Colomban, 1989; Colomban & Wey, 1997; Colomban, 2005). A big problem was the achievement of the right stoichiometry: silicon excess was very detrimental because of the relatively low temperature melting of silicon; on the other hand, carbon excess, not detrimental from the thermomechanical point of view, led to a great reactivity to air and to high electrical conductivity (Chauvet et al., 1992a; idem, 1992b; Mouchon & Colomban, 1996). However, the polymer precursors are linear macromolecules (1D) but SiC synthesis requires a 3D crosslinking. This was first achieved by Si-O-Si bridges but the oxygen atoms react with carbon excess at ~1200-1300°C (Karlin & Colomban, 1997; idem, 1998). The use of gamma irradiation for the crosslinking allows approaching better the stoichiometry and the thermal stability of SiC materials issued from polymeric precursor was increased (Ischikawa et al., 1991; Yang et al., 1991; Torecki et al., 1991; idem, 1992; Ischikawa, 1995; Ischikawa et al., 1998). Residual hydrogen atoms evolve above 1000°C whereas the free carbon created by the destruction of the methyl groups reacted with the Si-O group with the evolution of CO gas and forming new Si-C bonds above 1300°C, enhancing the crystallisation process.

Alternative route was developed by US Sacks' group (Torecki et al., 1992; Sacks et al., 1998): they used high-molecular-weight PCS. The infusible PCS was prepared by pressure pyrolysis of polydimethylsilane and the fibres formed by the dry spinning of concentrated PCS-based polymer solutions which were then pyrolysed in an inert atmosphere at 1000 to 1200°C.

The room temperature ultimate tensile strength ranges between 2.5 and 3.5 GPa as a function of the fibre grade with Young's modulus ranging between ~200 and 400 GPa, very close to the best properties achieved for bulk ceramics, films or crystals : ~430 GPa (Biswas et al., 2001; Dirras et al., 2004; Chung & Han, 2008). The axial room temperature thermal conductivity ranges between ~2-3 (oxygen rich, amorphous SiC) up to 50-60 W/mK for crystalline nearly stoichiometric SiC (Simon & Bunsell, 1984). The electrical conductivity from ~0.01 to 10 S.cm<sup>-1</sup> is highly related to the carbon content (Chauvet et al., 1992 a & b; Mouchon & Colomban, 1996). The reduction of the oxygen content in the fibres made by irradiating PCS produced fibres ~35% stiffer than the first generation fibres. The 1400°C creep rates are slightly improved (Sha et al., 2004). Actually the thermal stability in air remains poor for the first and 2<sup>nd</sup> generation SiC fibres, ca. ~1100°C. The third generation stoichiometric fibres exhibit properties much closer to those of bulk SiC but the thermal stability in air remains much lower than that of oxide fibers (Mouchon & Colomban, 1995; Colomban, 1997; Baxter et al., 2000, Ruggles-Wrenn & Kutsal, 2010; Ruggles-Wrenn & Whiting, 2011).

### 3. Polytypes

Polytypes are observed in a variety of covalent compounds where rotation along the covalent bond does not require a lot of energy. This often gives rise to more or less lamellar compounds with stacking faults along one direction: carbides (Feldmann et al., 1968; Salvador & Sherman, 1991; Choyke & Pensl, 1997), sulfides (CdS, ZnS, TiS<sub>2</sub>, ... (Kaflawi et al., 1969; Schneide & Kirby, 1972; Tronc et al., 1975; Moret & Huber, 1976; Lincot et al., 1997; Agrosi et al., 2009; Alvarez-Garcia et al., 2009; Chi et al., 2011), nitrides (Komatsu et al., 2010) but also some oxides (e.g. BaTiO<sub>3</sub> perovskites (Wu et al., 2006; idem, 2009)) and even diamond (Fayette et al., 1995; Bhargava et al., 1995).

As sketched in **Figure 1**, SiC structures consist of alternate layers of Si and C atoms forming a bi-layer. These bi-layers are stacked together to form face-centre cubic unit-cell (cubic stacking = ABC-ABC-ABC-, the so-called zinc-blende type cell, to be abbreviated c-SiC) or closed-packed hexagonal system (hexagonal stacking = AB-AB-AB-, the so-called wurzite cell, to be abbreviated h-SiC). Two consecutive layers form a bilayer which is named “h” (h for hexagonal) if it is deduced from the one below by a simple translation. If not, when an additional 180° rotation (around the Si-C bond linking the bilayers) is necessary to get the superposition, the bilayer is named “k” (for “kubic”). The “k” stacking is the reference of  $\beta$ -SiC cubic symmetry, only. The infinite combination of h/c stacking sequences led to hundreds of different polytypes (Feldman et al., 1968; Choyke & Pensl, 1997).

Very similar structures are known for many compounds. Formation of polytypes arises because the energy required to change from one type to the other is very low. Consequently, different structures can be formed during the synthesis, simultaneously, especially for layer materials (CdS, SiC, TiS<sub>2</sub>, MoS<sub>2</sub>, BN, AlN, talc, micas, illites, perovskites, see references above) including MBE superlattices (Yano et al., 1995). Polytypes structure consists of close packed planes stacked in a sequence which corresponds neither to the face-centered cubic system nor the close-packed hexagonal system but to complex sequences associating both cubic and hexagonal stackings, ones such as = -ABABCABAB-, or -ABCAABAB A-, or -ABABCABBA-, etc.).

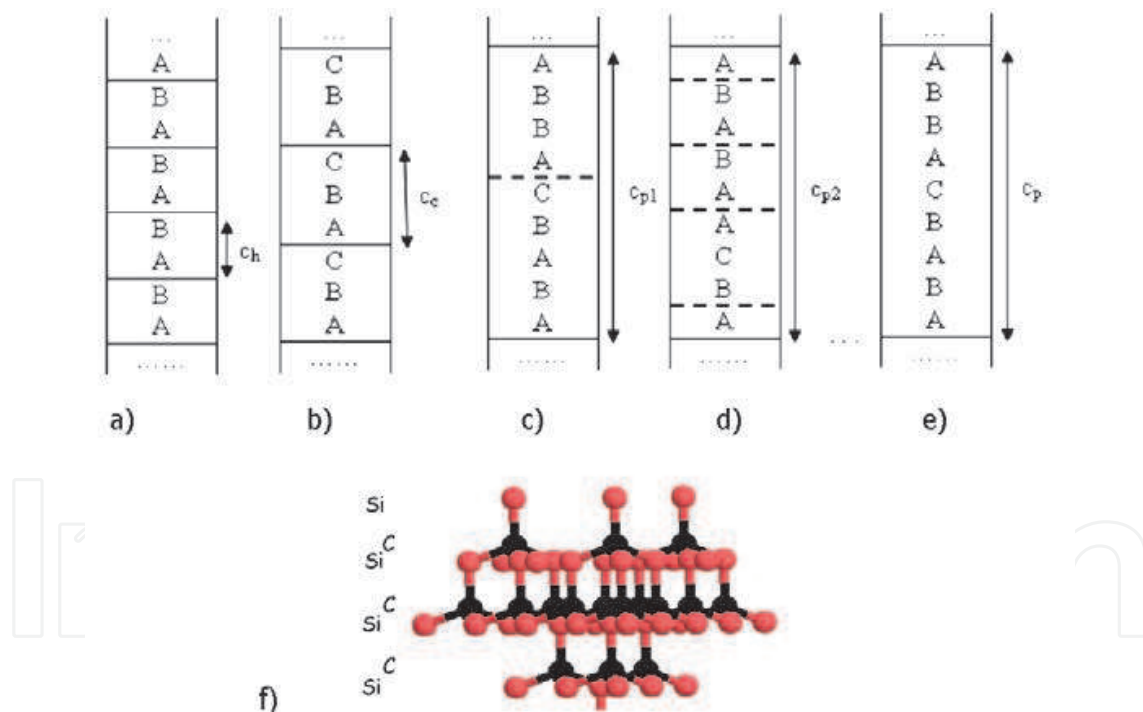


Fig. 1. Schematic diagrams of the (a) hexagonal, (b) cubic, (c,d) polytypes modifications and of the stacking fault disorder (e). SiC structures alternate layers of Si and C atoms to form a SiC bi-layer, AB or AC (e).

#### 4. From amorphous to crystalline materials

The precursor route led to a rather progressive transformation of a more or less 1D organised framework to a 3D amorphous one and subsequent thermal treatments control

the crystallization. The first problem to solve (Table 1) was the way to establish the bridge between the polymeric  $(\text{Si-C})_n$  chains: i) the first route (NLM<sup>TM</sup> Nippon Carbon fibre (Ishikawa, 1995)) is the thermal oxidation (Si-O-Si bridge) at relatively low temperature ( $\sim 200^\circ\text{C}$ ), the resulting  $\text{SiO}_2$  content decreases from  $\sim 25$  to  $\sim 10$  wt% with improvements), ii) the second one is the electronic irradiation that allows forming Si-C bridges but leads to a carbon excess ( $\text{C/Si} \sim 1.4$  in Hi-Nicalon<sup>TM</sup> Nippon Carbon fibre (Berger et al; 1995; idem, 1999); alternatively the grafting of Ti or Zr alkoxide (Ti or Zr addition) leads to rather similar material but the fibres could be made with smaller diameter (UBE Industries Tyranno<sup>TM</sup> LOX-M, ZE and TE grade fibres (Berger et al., 1997; idem, 1999); iii) the optimization of the organic precursor and associated thermal treatments gives stoichiometric SiC fibre (SA3<sup>TM</sup> Ube Industries, Sylramic<sup>TM</sup> Dow Corning Corp. Fibres and Hi-Nicalon<sup>TM</sup> Type S (Lipowitz et al., 1995; Ishikawa et al., 1998; Berger et al., 1999; Bunsell & Piant, 2006). The high temperature of the manufacture process leads to much larger grain sizes.

Generation	1 <sup>st</sup>	2 <sup>nd</sup>	3 <sup>rd</sup>			
Producer	Nippon Carbon	Nippon Carbon	Ube Industries	Ube Industries	Dow Corning Corp.	Nippon Carbon
Grade	NLM Nicalon	Hi-Nicalon	ZE,TE	SA3	SYLRAMIC	Hi-S
Reticulation	Si-O bond	Electron irradiation	Electron irradiation	Si-O bond	Si-O bond	Electron irradiation
Grain size/ nm	$<2$	5-10	5-10	$<50$	$<50$	$<50$
Si/C stoichiometry	1.3	$<1.3$	$<1.3$	$\sim 1$	$\sim 1$	$\sim 1$
Diameter / $\mu\text{m}$ (+/- 3)	15	12	11	7.5	10	12

Table 1. Small diameter SiC fibre generations.

The first generations fibre microstructures consist of an amorphous ternary phase made of  $\text{SiO}_x\text{C}_y$  tetrahedra (Porte & Sartre, 1989) with  $x+y = 4$ , with  $\sim 1.4$ - $1.7$  nm SiC crystallites and  $\sim 5\%$  of randomly oriented free carbon aggregates, 1 nm in size (Nicalon<sup>TM</sup> 200 grade,  $x=1.15$ ). Carbon (002) lattice fringe images showed small stacks of two fringes of around 0.7 nm in size suggesting that the basic structural unit (BSU) was a face-to-face association of aromatic rings, called dicoronenes, in which the hydrogen-to-carbon atomic ratio is 0.5. Accordingly, a porosity level of 2% was present (Le Coustumer et al., 1995 a & b). Other studies proposed that the intergranular phase should be written as  $\text{SiO}_x\text{C}_{1-x/2}$ , which suggests that the composition varies continuously from SiC to  $\text{SiO}_2$  as the oxygen traces varied (Bodet et al., 1995). The removal of oxygen from the cross-linking process resulted in a stoichiometry closer to  $\text{Si/C} = 1$  and an increase in size of the  $\beta$ -SiC grains which were in the range of 5 to 10 nm in commercial fibres. The TEM images show well ordered SiC

surrounded by highly disordered/amorphous SiC interphase and free carbon grains (Monthieux et al., 1990; idem, 1991; Havel, 2004; Havel et al., 2007).

### 5. How to identify the polytypes, the stacking disorder and the relative proportion of each polytypes?

The challenge for the nanotechnologies, which is to achieve perfect control on nanoscale related properties, requires correlating the production conditions to the resulting nanostructure.

Transmission electron microscopy (darkfield and high resolution images, electronic diffraction, etc. (see e.g. Mirguet et al., 2009; Sciau et al., 2009)) is the most efficient technique to determine the grain size, the defaults (disorder, superstructures, amorphous interface, voids, etc.) but the technique is destructive, time-consuming and may modify the sample structure. Moreover the representativity of the samples is always poor.

Raman spectrometry is a very interesting technique to study nanomaterials since it investigates the matter at a sub-nanometer scale, i.e. the scale of the chemical bonds. The automatic mapping (best spatial resolution  $\sim 0.5$  to  $1 \mu\text{m}^2$  as a function of objective aperture and laser wavelength) allows a very representative view of the sample surface. Each Raman peak corresponds to a specific vibration (bending, stretching, librational, rotational and lattice modes) of a given chemical bond, and provides information (even on heterogeneous materials, e.g. composites) such as the phase nature and symmetry, distribution, residual stress,... (Colomban, 2002; Gouadec & Colomban, 2007). Since the Raman scattering efficiency depends on the polarisability of the electronic cloud, it can be very sensitive to light elements involved in covalent bonds (C, H, N, B, O, ...), which is a valuable advantage, when compared to X-ray/electron-based techniques (EDS, micro-probe,...). In the case of coloured materials if the exciting laser energy is close to that of absorbing electronic levels, resonance Raman scattering occurs and the technique becomes a surface analysis in the range of  $\sim 20$  to  $100 \text{ nm}$  in-depth penetration (also depending on the wavelength, (Gouadec & Colomban, 2007)). Then, the selection of a given wavelength allows probing specific layers. The main advantages compared to infrared spectrometry are that the laser in a Raman equipment can be focused down to  $\sim 0.5$ - $1 \mu\text{m}^2$ , allowing for imaging specific areas (Gouadec et al, 2001; Colomban, 2003; idem, 2005) and that Raman peaks are narrower than IR bands (Gouadec & Colomban, 2007 and references herein).

**Fig. 2a** shows the representative electronic diffraction pattern ([2-1-10] axis) of a SA3™ fibre thermally treated at  $1600^\circ\text{C}$  in inert atmosphere. Most of the Bragg spots correspond to 6H SiC (hexagonal  $P6_3mc$  space group), i.e. to the most simple polytype (Fig. 1). The diffuse scattering along the horizontal axis ([01-11], arises from the stacking disorder of the SiC bilayer units. On the contrary, the disorder signature is weaker on the X-ray diffraction pattern (small polytype peak at  $d = 0.266 \text{ nm}$ , **Fig. 2b**). However Bragg diffraction highlights the most crystalline part and sweeps the information on low crystalline (e.g. carbon) second phases. Fig. 3 shows the corresponding Raman spectra. For 1<sup>st</sup> and even 2<sup>nd</sup> generation fibres the Raman spectrum is dominated by the carbon doublet that overlaps the SiC Raman fingerprint. Specific thermal and chemical treatments are necessary to eliminate most of the carbon second phases and thus to have access to the Raman signal of the SiC phases (Havel & Colomban, 2005).

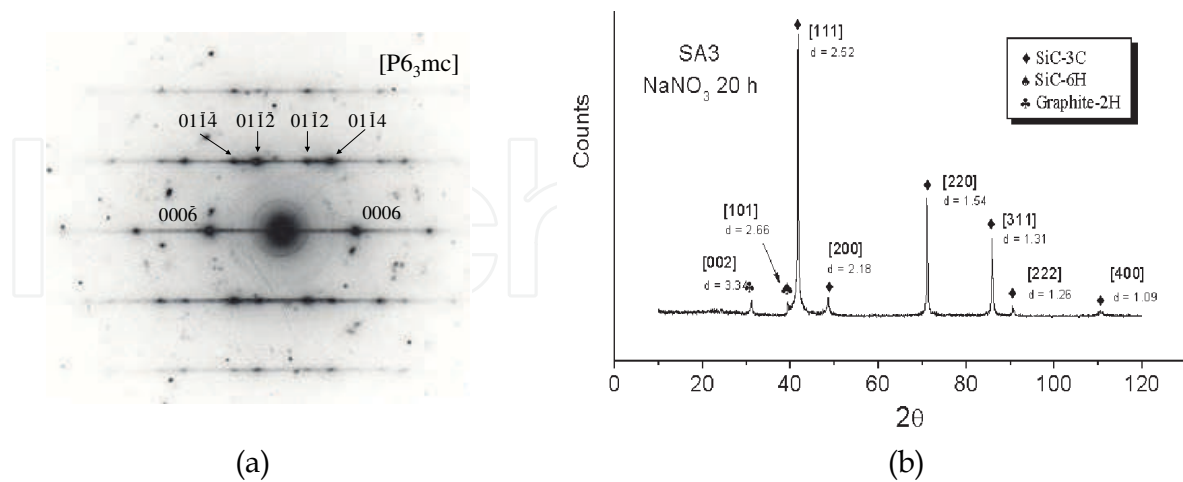


Fig. 2. a) Representative electron diffraction pattern recorded on SA3<sup>TM</sup> (Ube Industries Ltd, see Table 1) fibre thermally treated at 1600°C under inert atmosphere (Courtesy, L. Mazerolles); b) X-ray diffraction pattern recorded on powdered SA3<sup>TM</sup> fibre (the immersion in molten NaNO<sub>3</sub> do not modify the pattern, (Havel & Colombari, 2005)).

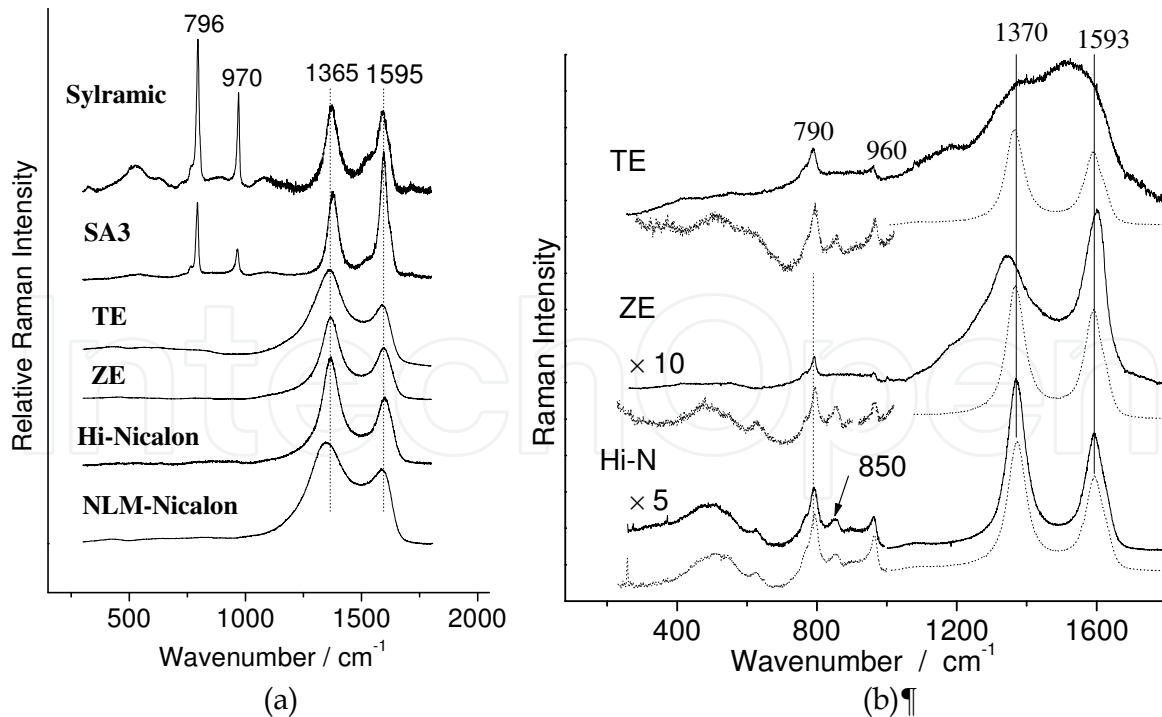


Fig. 3. Representative spectra of the as-produced fibres (a) and after different thermal/chemical treatments in order to highlight the SiC fingerprint (b).



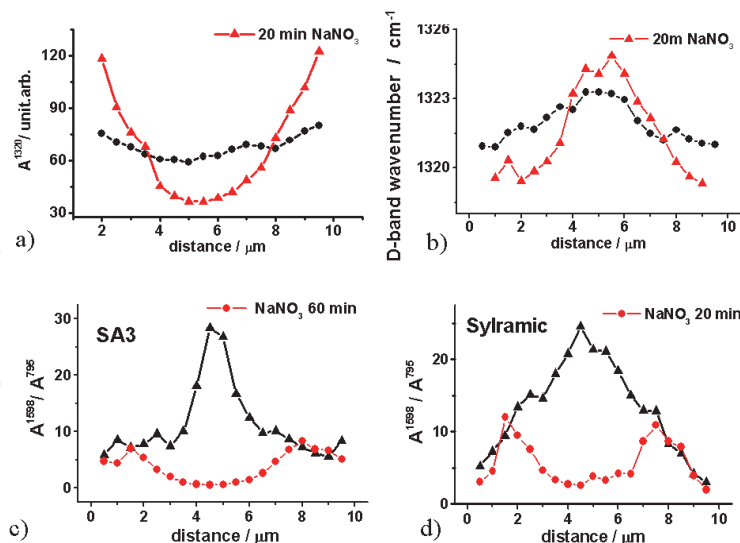


Fig. 4. Variations of a) the  $\sim 1320 \text{ cm}^{-1}$  Raman peak area ( $A^{1320}$ ) and b) its wavenumber shift across the diameter of a NLM™ fibre polished section, as-received (dot) and after a chemical attack (triangle) eliminating the carbon phase; a comparison of the variation of the "carbon rate" (Raman peaks surfaces ratio  $A^{1598} / A^{795}(\text{C/SiC})$ ) along the diameter of SA3™ (c) and Sylramic™ fibres section (d) ( $\lambda = 632 \text{ nm}$ ,  $P = 0.5 \text{ mW}$ ,  $t = 60 \text{ s}$ ).

Raman peaks attribution of the disordered carbons present in SiC fibres has been previously discussed (Karlin & Colombar, 1997; idem, 1998; Gouadec et al., 1998). Pure diamond ( $\text{sp}^3$  C-C bonds) and graphite (in plane  $\text{sp}^2$  C=C bond) have sharp stretching mode peaks at  $1331$  and  $1581 \text{ cm}^{-1}$  respectively. The two main bands of amorphous carbons are then assigned to diamond-like (D band for diamond and disorder) and graphite-like (G band for graphite) entities. Because diamond Raman scattering cross-section is much lower than that of graphite ( $\sim 10^{-2}$ ), a weak  $\text{C}_{\text{sp}^3}\text{-C}_{\text{sp}^3}$  stretching mode is expected. Actually, given the small size of carbon moieties and the strong light absorption of black carbons the contribution of the chemical bonds located near their surface will be enlarged (resonance Raman, the Raman wavenumbers shift with used laser wavelength, see in (Gouadec & Colombar, 2007)). The D band corresponds to vibration modes involving  $\text{C}_{\text{sp}^3}\text{-C}_{\text{sp}^2/\text{sp}^3}$  bonds also called  $\text{sp}^{2/3}$ . This band presents a strong resonant character, evidenced by a high dependence of the intensity and position on wavelength. Additional components below  $1300 \text{ cm}^{-1}$  arise from hydrogenated carbons and those intermediate between D and G bands have been assigned to oxidised and special carbon phases (Karlin & Colombar, 1997; idem, 1998; Colombar et al., 2002). The wavenumber of the  $\text{sp}^3$  carbon bond (D peak) measures the aromaticity degree (aromaticity is a function of the "strength and extension size" of the  $\pi$  electronic clouds and thus also function of the crystal order) and hence is directly related to the electric properties of the material (Mouchon & Colombar, 1996). This value depends directly on the thermal treatment temperature history and hence is also related to the mechanical properties, see details in (Gouadec & Colombar, 2001; Colombar, 2003).

The plot of the carbon fingerprint parameters recorded across the fibre section diameter (on fracture) shows the very anisotropic carbon distribution (Fig. 4). Chemical treatments eliminate the carbon in the analysed SiC volume and hence allow a better study of the SiC phases (Havel & Colombar, 2005).

The Raman spectrum of well crystallised SiC phases is observed between 600 and 1000  $\text{cm}^{-1}$  (Feldman et al., 1968; Nakashima et al., 1986; idem, 1987; idem, 2000; Nakashima & Hangyo, 1991; Nakashima & Harima, 1997; Okimura et al., 1987; Tomita et al., 2000; Hundhausen et al., 2008.). The main Raman peaks centred at 795 and 966  $\text{cm}^{-1}$  correspond to the transverse (TO) and longitudinal (LO) optic modes respectively of the (polar) cubic 3C phase, also called  $\beta$  SiC. Any other definite stacking sequence is called  $\alpha$ -SiC and displays either hexagonal or rhombohedral lattice symmetry. Polytypes in the  $\alpha$ -SiC structure induce the formation of satellite peaks around 766  $\text{cm}^{-1}$  and of additional features between the TO and LO modes (Figs 5 & 6). However, the TO mode is twice degenerated; while  $\text{TO}_1$  is centred at 796  $\text{cm}^{-1}$ ,  $\text{TO}_2$  is a function of the “h” layers concentration in the structure. A linear variation of 0.296  $\text{cm}^{-1}/\%$  has been demonstrated (Salvador & Sherman, 1991; Feldman et al., 1968).

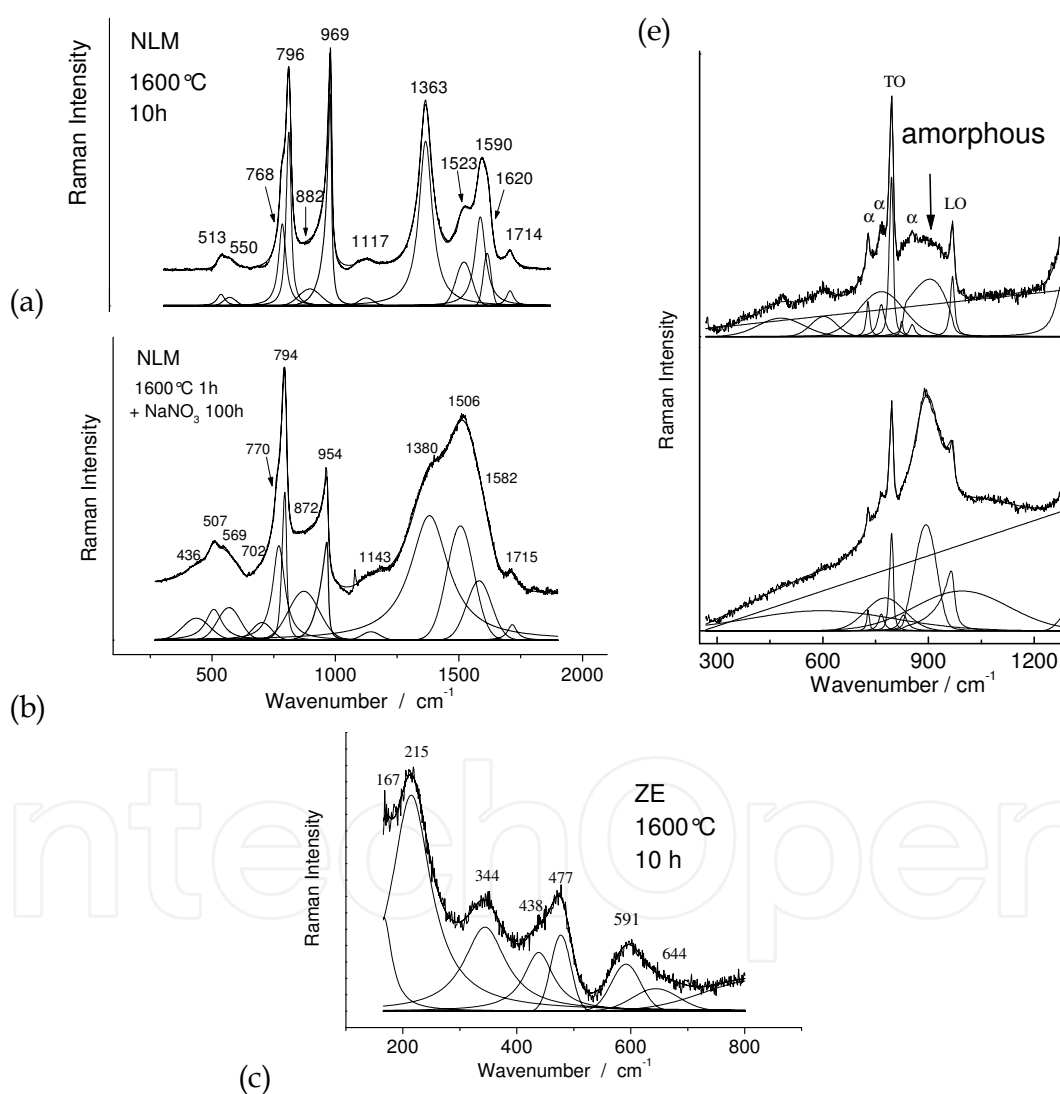


Fig. 5. Representative Raman spectra recorded for NLM<sup>TM</sup> Nicalon fibres thermally and chemically treated (a,b). Detail on the disorder-activated acoustic modes observed for ZE<sup>TM</sup> fibre (c) and for very amorphous SiC zone are shown.

The main effect of the disorder is the break of the symmetry rules that excludes the Raman activity of the vibrational, optical and acoustical, modes (phonons) of the whole Brillouin

zone: only zone centre modes give rise to a Raman activity. Because the wavenumber of these modes shift with wavevector value, they give broad asymmetric bands. Fig. 6 illustrates the apparition of satellite peaks because the step-by-step Brillouin Zone folding associated to the formation of polytypes. On the contrary, stacking disorder lead to a projection of the vibrational density of state on the vertical energy axis and broad asymmetric bands are observed.

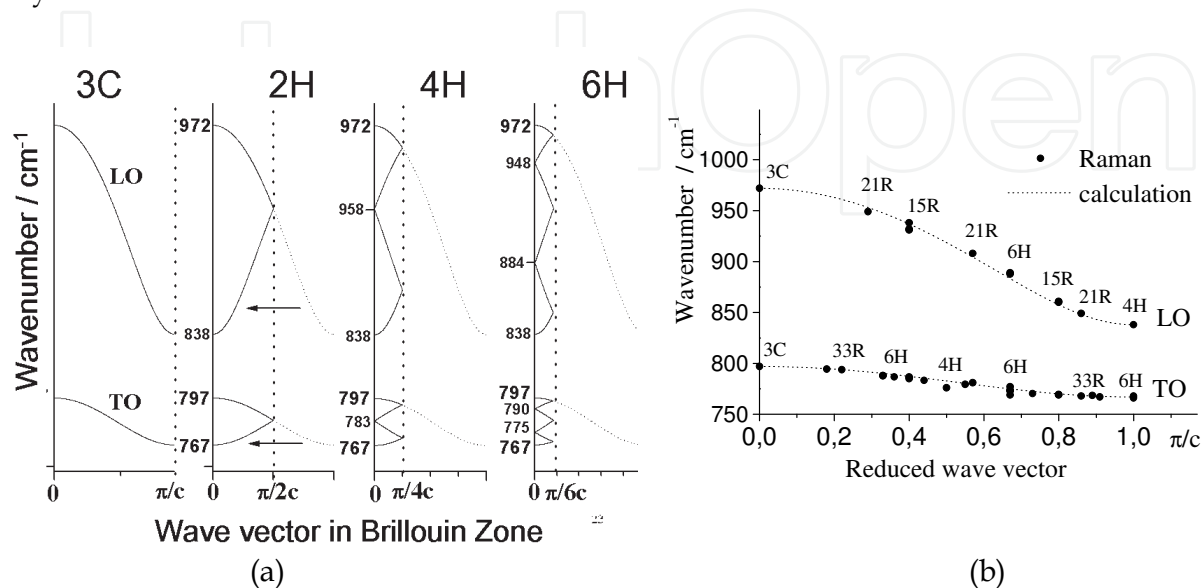


Fig. 6. a) Sketch of the folding of the original phonon Brillouin zone in the stretching LO/TO mode region along the stacking axis of the reference cubic symmetry by factor 2 (2H polytype), 4 (4H) and 6 (6H). b) Satellite peak wavenumbers for series of polytypes (after Nakashima & Harima, 1997).

The comparison of the Figures 2a (Diffraction & diffuse scattering) and 2b (Raman scattering) points out the very different sensitivity of these two methods. Fig. 4 compares the Raman spectra of the different generation SiC fibres, with carbon excess ranging from ~20 wt% (1<sup>st</sup> generation) to less than 1 wt% (3<sup>rd</sup> generation). A small wavenumber shift may be associated to the change of the exciting wavelength. Another important point is that for coloured materials, the interaction between laser light and matter must be very strong and hence the light absorption. This may have detrimental effect (local heating – and thermal induced wavenumber shift – (Colomban, 2002), oxidation and phase transition (Gouadec et al., 2001) in the lack of attention but this also controls the penetration depth of the laser light: the penetration can be limited to a few (tenths of) nanometers (Gouadec & Colomban, 2007).

Figs 5 to 9 give examples of the variety of Raman signatures observed on SiC materials issued of the organic precursor routes.

The narrow peaks pattern of crystalline polytypes is obvious and assignments are univocal with the comprehensive work of Nakashima (Nakashima et al., 1986; idem, 1987; Nakashima & Harima, 1997), see Fig. 6. The most stringent new features are the very broad bands observed at ~730 and 870 cm<sup>-1</sup> and the structured pattern below 600 cm<sup>-1</sup>. The first feature corresponds to the amorphous silicon carbide and the second one to the acoustic modes rendered active because of the very poor crystallinity of the fibre.

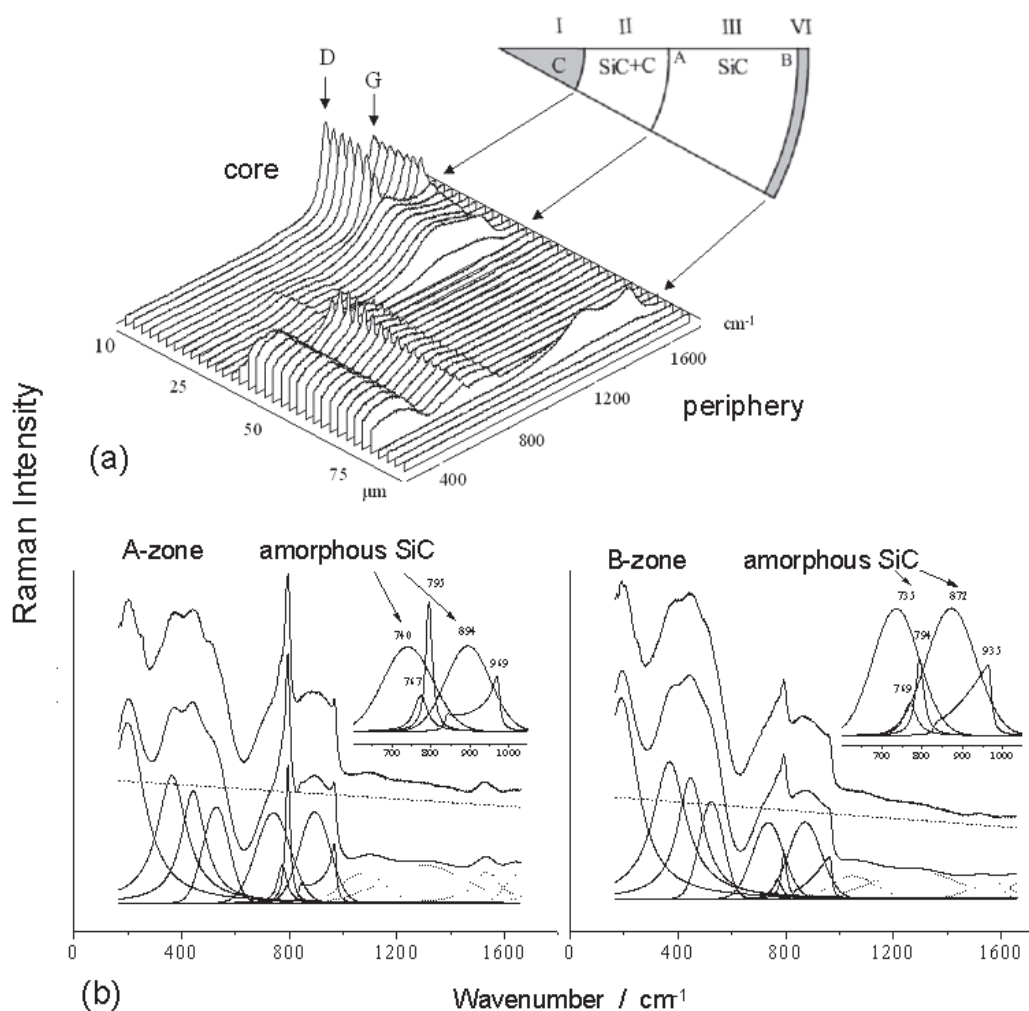


Fig. 7. a) Raman spectra recorded every  $2\mu\text{m}$  along a line from the centre of a SCS-6 Textron<sup>TM</sup> fibre ( $L=532\text{nm}$ ,  $1\text{mW}$ ,  $120\text{s/spectrum}$ ); b) representative spectra of the pure SiC (III) zone; the different components have been fitted with Gaussian or Lorentzian lines: the broad  $740$  and  $894\text{ cm}^{-1}$  bands correspond to amorphous SiC, the  $767\text{ cm}^{-1}$  to 6H-SiC and the  $795\text{ cm}^{-1}$  band to 3C-SiC polytypes.

The apparition of disordered activated acoustic phonon in the Raman spectrum is not surprising in compounds with large stacking disorder (Chi et al., 2011). Additional multiphonon features are not excluded. However, many Raman studies of such materials have been made using exciting laser line leading to a resonance spectrum, simpler, in which the contribution of the disordered activated modes is low or even not detected.

Very similar features are observed for SiC materials prepared by Chemical Vapour Infiltration. The Raman spectra of the SiC coating deposited on a small diameter ( $\sim 7\mu\text{m}$ ) carbon fibre core to obtain the SCS-6 Textron<sup>TM</sup> fibre, a  $\sim 120\mu\text{m}$  thick fibre used to reinforce metal matrix consist in features where the acoustic phonon intensity becomes stronger than the optical ones. Furthermore the latter group is dominated by the broad bands of the amorphous SiC.

Because of the different laser line absorption, Rayleigh confocal imaging allows to have very interesting image of the heterogeneous material (Colomban & Havel, 2002; Colomban, 2003; Havel & Colomban, 2003; idem, 2004; idem, 2005; idem, 2006). Fig. 8 shows representative spectra recorded on the deposit obtained around the fibres of a textile perform. In order to

optimise the thermomechanical properties of the composite a first coating of the SiC fibre with BN has been made. The spectra show the 3C (narrow peak at 799 and 968  $\text{cm}^{-1}$ ), 6H (786  $\text{cm}^{-1}$ ), 8H or 15R (768  $\text{cm}^{-1}$ ) as well the broad and strong contribution of amorphous SiC (optical modes at 750 & 900  $\text{cm}^{-1}$  and acoustic modes at 450  $\text{cm}^{-1}$  with shoulder at 380 and 530  $\text{cm}^{-1}$ ). Traces of carbon (1350-1595  $\text{cm}^{-1}$  doublet) are also observed. We assign the broad Gaussian peaks at  $\sim 700 \text{ cm}^{-1}$  and  $\sim 882 \text{ cm}^{-1}$  to the amorphous SiC. Indeed, the position of the band at ca 882  $\text{cm}^{-1}$  is exactly between the two optical modes at a wavenumber of  $(796+969) / 2 = 882.5 \text{ cm}^{-1}$ . Dkaki et al. (Dkaki et al., 2001) already assigned the band at ca. 740  $\text{cm}^{-1}$  to the amorphous SiC phase.

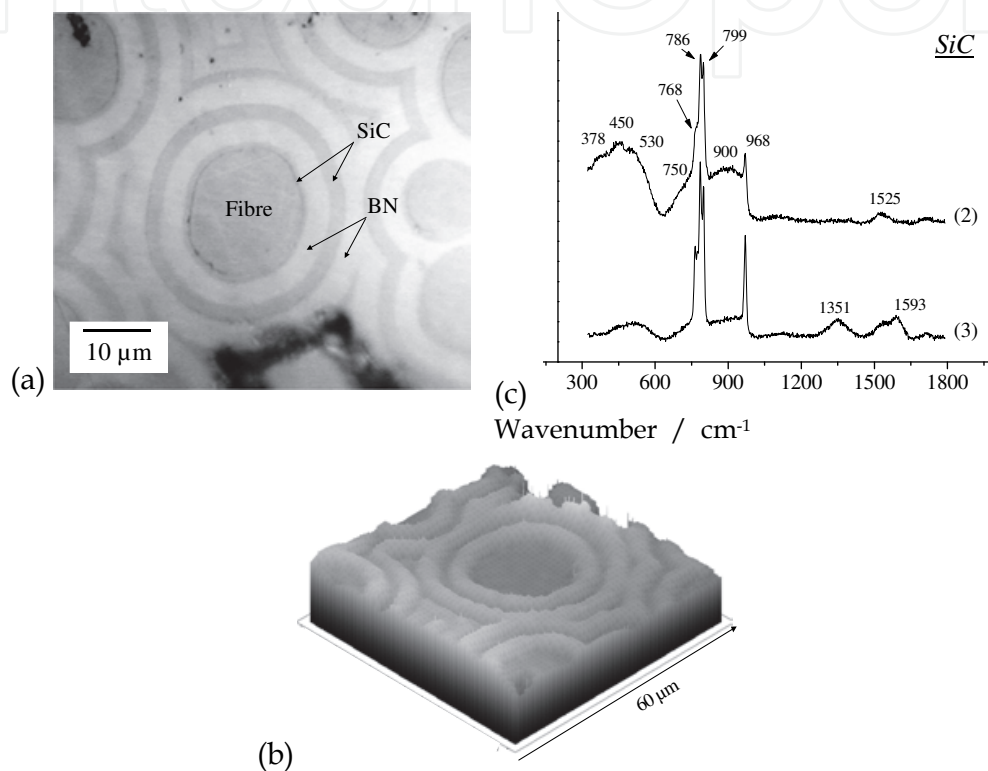


Fig. 8. Optical photomicrograph (a) and Rayleigh image (b) of a SiC (BN coated) fibre reinforced-SiC matrix composite. Examples of SiC spectra are given in c). Polytypes are evidenced by 786 (4H) and 768 (6H)  $\text{cm}^{-1}$  TO modes. The fingerprints of 3C (799  $\text{cm}^{-1}$ ) and amorphous (900  $\text{cm}^{-1}$  broad band) SiC are also present.

When classically used, a Raman spectrometer is built to avoid the elastic (Rayleigh) scattering which is much more intense ( $\times 10^6$ ) than the inelastic one (Raman) and masks it. However, the Rayleigh signal contains useful information (volume of interaction and dielectric constant) that can be recorded in only few seconds, giving rise to topological and/or chemical maps (a high resolution Raman image requires tenths of hours!). The combination of Rayleigh image and Raman scattering is very interesting to study indentation figures (Colomban & Havel, 2002). Rayleigh scattering gives image of the topology mixed with information on the chemical composition through the variation of the optical index. Fig. 9 presents the Rayleigh image of the Vickers indented zone of the mixed SiC+C region (zone II) of a SCS-6 polished section (see Fig. 7). The automatic XY mapping has been performed with an objective with an Z axis extension of the focus volume sufficiently large to be bigger than the indentation depth. Thus, a 3D view is obtained. The

up-deformation of the fibre matter close to the edges resulting from the pyramidal shape of the Vickers indenter is obvious. The residual stress is calculated using the experimental relationship previously established under pressure (Salvador & Sherman, 1991; Olego et al., 1982). The amorphization is obvious at the center of the indented area with the relative increase of the intensity of the 760-923  $\text{cm}^{-1}$  doublet and the decrease of the TO/LO doublet; note, the up-shift of the TO mode from 796 to 807  $\text{cm}^{-1}$ . Similar information can be extracted from the D carbon band using the relationship established by Gouadec & Colombar, 2001.

Peak	Out of the indented area		At the tip position	
	$\bar{\nu}$ ( $\text{cm}^{-1}$ )	P (GPa)	$\bar{\nu}$ ( $\text{cm}^{-1}$ )	P (GPa)
TO	$796 \pm 2$	0	<b><math>807 \pm 6</math></b>	<b><math>3 \pm 2</math></b>
LO	$969 \pm 2$	0	$969 \pm 4$	$3 \pm 2$
D	$1351 \pm 3$	0	$1369 \pm 4$	<b><math>3 \pm 1</math></b>

Table 2. Comparison between the TO/LO peak wavenumbers measured at the tip and out of the 50 g Vickers indented area on SCS-6 Textron™ fibre, mixed SiC-C zone II (see Fig. 7a).

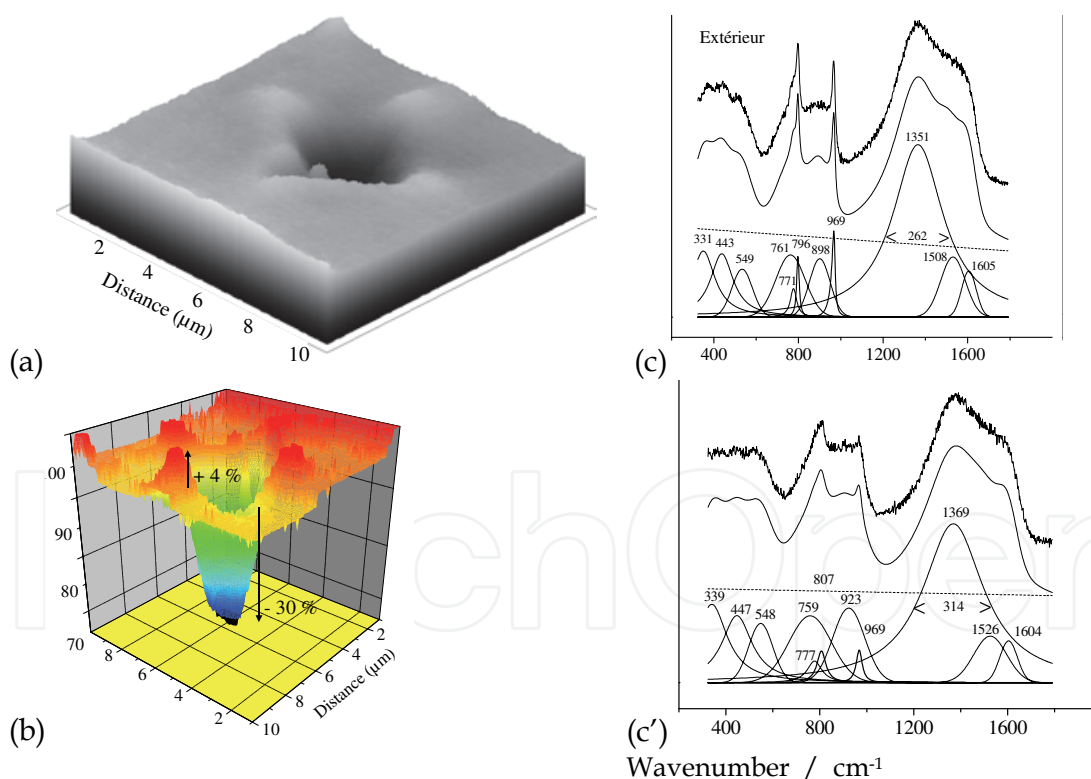


Fig. 9. (a,b) Rayleigh images of the Vickers indented area on the mixed SiC+C II region of a SCS-6 Textron™ fibre (100x100 spectra, 3s/Spectrum,  $10^{-6}$  mW,  $\lambda = 532$  nm); c,c') representative spectra (step:  $0.1\mu\text{m}$ ) recorded at the core (c') and the periphery (c) of the indented area; the fitting of the different component allows calculating the residual hydrostatic pressure (see Table 2).

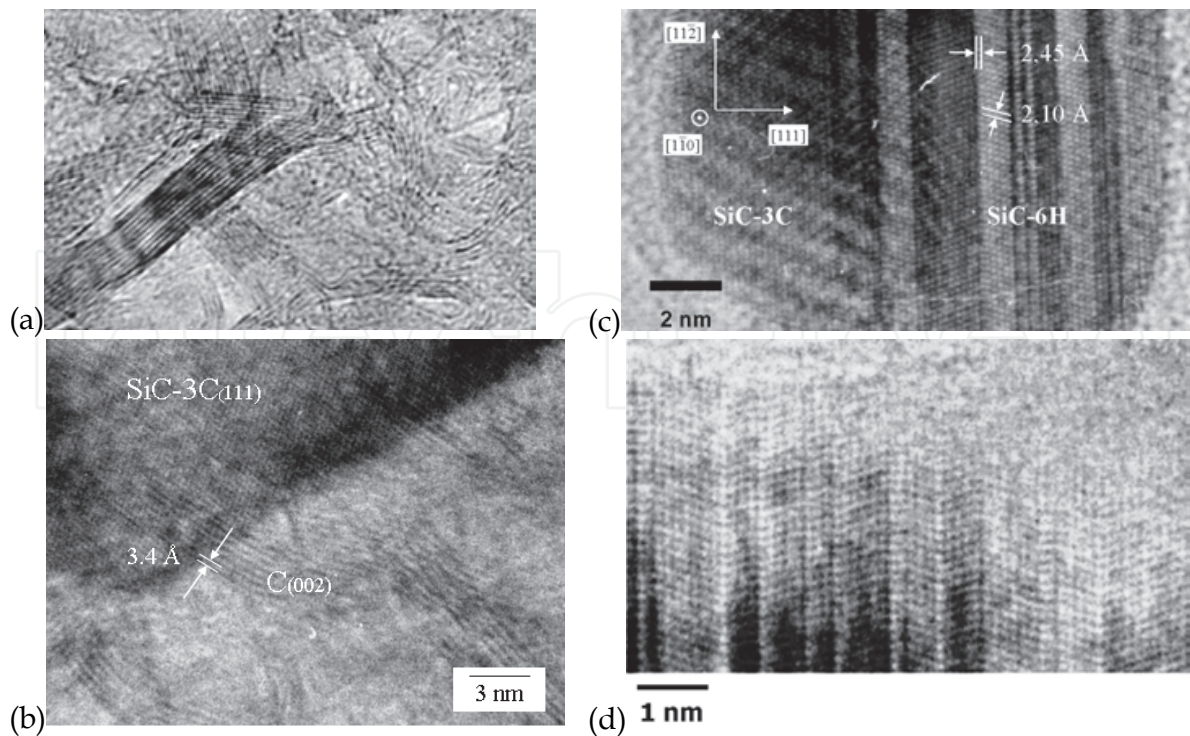


Fig. 10. TEM photomicrographs showing the carbon slabs in 1600°C thermally treated SA3 fibre (a,b) and the extension of the polytypes in thermally treated NLM 202™ (c) and SA3™ (d) fibres. The progressive transition between crystalline layers and amorphous zone is shown in (d) (Courtesy, L. Mazerolles).

## 6. Microstructure and defects

Fig. 10 shows representative high resolution Transmission Electron Microscopy (TEM) images recorded on thermally treated NLM 202 Nicalon™ and SA3™ fibres (Table 1). Structural studies of SiC nanocrystals were carried out on fragments of fibres deposited on a copper grid after crushing in an agate mortar (Havel, 2004; Havel et al., 2007). In SA3™ fibre the carbon phase appears to be well organized, graphitic, according to the narrow doublet of the Raman spectra (Fig. 3a). The interplane spacing is 0.33 nm. The stacking sequence of SiC bilayers is clear in Fig. 10c & d, because the contrast jump relative to the Bragg peak shifts. The domain sizes along the stacking direction might reach 3-4 nm. Figure 10c shows a typical HRTEM image of a nanocrystal with a size of 15 nm along its longest axis consisting of two regions corresponding to the  $\alpha$  and  $\beta$  phases. The stacking faults, which are clearly seen on the micrograph, show no periodicity along the c axis of the hexagonal structure. Stacking faults can be considered as a perturbation of the  $\beta$ -SiC 3C stacking sequence so that the  $\alpha$  phase can be seen as a sequence of  $\beta$ -SiC domains of various sizes ranging from 0.2 to 5 nm. The progressive transition between crystalline domains explains the variety of Raman fingerprint. There is a good agreement between Raman and TEM data.

## 7. Quantitative extraction of the (micro)structural information present in the Raman spectrum

For the decomposition of the SiC Raman peaks we used the spatial correlation model (SCM), which was established by Richter et al. (Richter et al., 1981), and by Nemanich et al.

(Nemanich et al., 1981) and then popularised Parayantal and Pollack (Parayantal & Pollack, 1984). A comprehensive description for non-specialist has been given in our previous work (Gouadec & Colombar, 2007). It can be briefly explained as follows. In "large" crystals, phonons propagate "to infinity" and because of the momentum selection rule the first order Raman spectrum only consists of "q=0" phonon modes, i.e. the centre of the Brillouin Zone (Fig. 6). However, since crystalline perfection is destroyed by impurities or lattice disorder, including at the surface where atoms environment is singular, the phonon function of polycrystals is spatially confined. This results in an exploration of the wavevectors space and subsequent wavenumber shifts and band broadening. Another effect is the possible activation of "symmetry forbidden" modes. This is linked to the Brillouin zone folding as illustrated in Fig. 6. In the 6H polytype structure, the zone is folded three times at the  $\Gamma$  centre point and the reduced wave vectors that can be observed are at  $q = 0, 0.33, 0.67$  and  $1$  (Feldman et al., 1968; Nakashima et al., 1987; Nakashima & Harima, 1997). The Raman line broadening can be described by the (linear) dependence of its half width upon the inverse grain size, as reported previously for many nanocrystalline materials including  $\text{CeO}_2$  (Kosacki et al., 2002), BN (Nemanich et al., 1981), Si (Richter et al., 1981), etc.

In equation (1), the SCM describes the crystalline quality by introducing a parameter  $L_0$ , the coherence length, which is the average extension of the material homogeneity region. Noting  $q$  the wave vector expressed in units of  $\pi/a$  ( $a$  being the lattice unit-cell parameter) and  $\Gamma_0$  the half width of Raman peaks for the ordered reference structure, the intensity  $I(\bar{\nu})$  at the wavenumber  $\bar{\nu}$  is then given by equation (2). (Richter et al., 1981; Nemanich et al., 1981; Gouadec & Colombar, 2007).

The exponential function represents a Gaussian spatial correlation and  $\bar{\nu}(q)$  is the mode dispersion function, which can be deduced from neutron scattering measurements or from calculations often based on a rigid-model structure (Parayanthal & Pollak, 1984; Weber et al., 1993; Kosacki et al., 2002).

$$I(\bar{\nu}) = I_0 \times \int_{q=0}^{q=1} e^{-\frac{k_{BZ}^2 \times (q-q_0)^2 \times L_0^2}{16 \times \pi^2}} \times \frac{dq}{[\bar{\nu} - \bar{\nu}(q)]^2 + \left(\frac{\Gamma_0}{2}\right)^2} \quad (1)$$

While the one dimensional disorder (in the stacking direction) leads to the polytypes formation, a complete disorder induces the total folding of the Brillouin zone and the apparition of a very broad Raman signal (density of state spectrum, e.g. Fig. 9c). The phonon confinement is observed for small grains in a well crystallized state.

The dispersion curve can be modelled with the Eq. 2-4 (Parayanthal & Pollak, 1984). Our 6H reference corresponds to coefficients  $A$  and  $B$  of respectively  $3.18 \times 10^5$  and  $1.38 \times 10^{10}$  for TO and  $4.72 \times 10^5$  and  $8.52 \times 10^{10}$  for LO modes (Havel & Colombar, 2004).

$$\bar{\nu}(q) = \sqrt{A + \sqrt{A^2 - B \times (1 - \cos(\pi q))}} \quad 0 \leq q \leq 1 \quad (2)$$

with

$$A = \frac{1}{2} \times \bar{\nu}_{(q=0)}^{-2} \quad (3)$$



and

$$B = \frac{1}{2} \times \mathbf{v}_{(q=1)}^{-2} \times \left( \mathbf{v}_{(q=0)}^{-2} - \mathbf{v}_{(q=1)}^{-2} \right) \quad (4)$$

The SCM has been used to determine the size and structure of SiC nanocrystals extracted from annealed SiC fibre. The Raman spectra of the NLM fibres annealed 1h and 10h are shown in Fig 5. The SiC Raman signature, is composed of the 2 optical TO and LO modes. A satellite at 768 cm<sup>-1</sup> indicates the presence of the 6H-SiC polytype (Fig. 6). The most interesting parameter in this SiC signature is the strong asymmetry of the LO peak at ~ 969 cm<sup>-1</sup> (see also Fig. 7). The TO peak is much less asymmetric and centred at 796 cm<sup>-1</sup>. The elementary peaks obtained from the decomposition of the experimental spectrum are shown in Fig. 5 and the adjustment parameters (position, q<sub>0</sub> and L<sub>0</sub>) are summarized in Table 3. Note that the accuracy on the calculated reduced wavevector, q<sub>0</sub>, is increased for the LO mode because its dispersion curve explores a wider wavenumber range (838-972 cm<sup>-1</sup>) than the TO mode (767-797 cm<sup>-1</sup>).

Peak	Parameter	1h	10h	1h + corroded
TO	$\bar{\mathbf{V}}$ (cm <sup>-1</sup> )	796.8	795.6	794.2 ± 2
	q <sub>0</sub>	0.22 ± 0.02	0.26 ± 0.01	0.30 ± 0.01
	L <sub>0</sub> (nm)	5.6 ± 1.5	6.5 ± 1.2	5.6 ± 0.6
LO	$\bar{\mathbf{V}}$ (cm <sup>-1</sup> )	961.7	969.5	954.5
	q <sub>0</sub>	0.18 ± 0.03	0.00 ± 0.07	0.26 ± 0.01
	L <sub>0</sub> (nm)	2.9 ± 0.4	3.8 ± 0.9	5.2 ± 0.5

Table 3. Peak fitting parameters of the TO and LO peaks of SiC calculated from the Raman spectra of the NLM fibres annealed 1h and 10h at 1600°C and annealed 1h then corroded 100h in NaNO<sub>3</sub> (Havel & Colombar, 2005).

For the fibre annealed for 1h, the L<sub>0</sub> parameters of both TO and LO peaks show a confinement dimension in the range of 2.5 to 7 nm, in good agreement with the TEM image. After 10h annealing, the TO and LO peaks become sharper and more intense, indicating an increase in the size of the nanocrystals. This is confirmed by the L<sub>0</sub> parameter, which gives a confinement dimension slightly higher, between 3 and 8 nm, according to the polytype domain size (Fig. 10).

## 8. Raman imaging

Raman imaging is very powerful, especially for heterogeneous materials but its rise is limited because of a lack of real control on the x, y, z spatial resolution (changing the diameter of confocal hole allows however some possibility) and of the huge recording time required (the spectrometer has often to be used during night time). However, a precise study of the laser shape, can improve the control on the resolution and since the CCD detectors are more and more sensitive, Raman images will now require more reasonable acquisition time (hours!). Note, that once the image is recorded, the set of spectra (also called hyperspectrum) has to be

analysed, which is much more time-consuming than the acquisition itself. This is why automatic decomposition software must be developed (Havel et al., 2004; Gouadec et al., 2011).

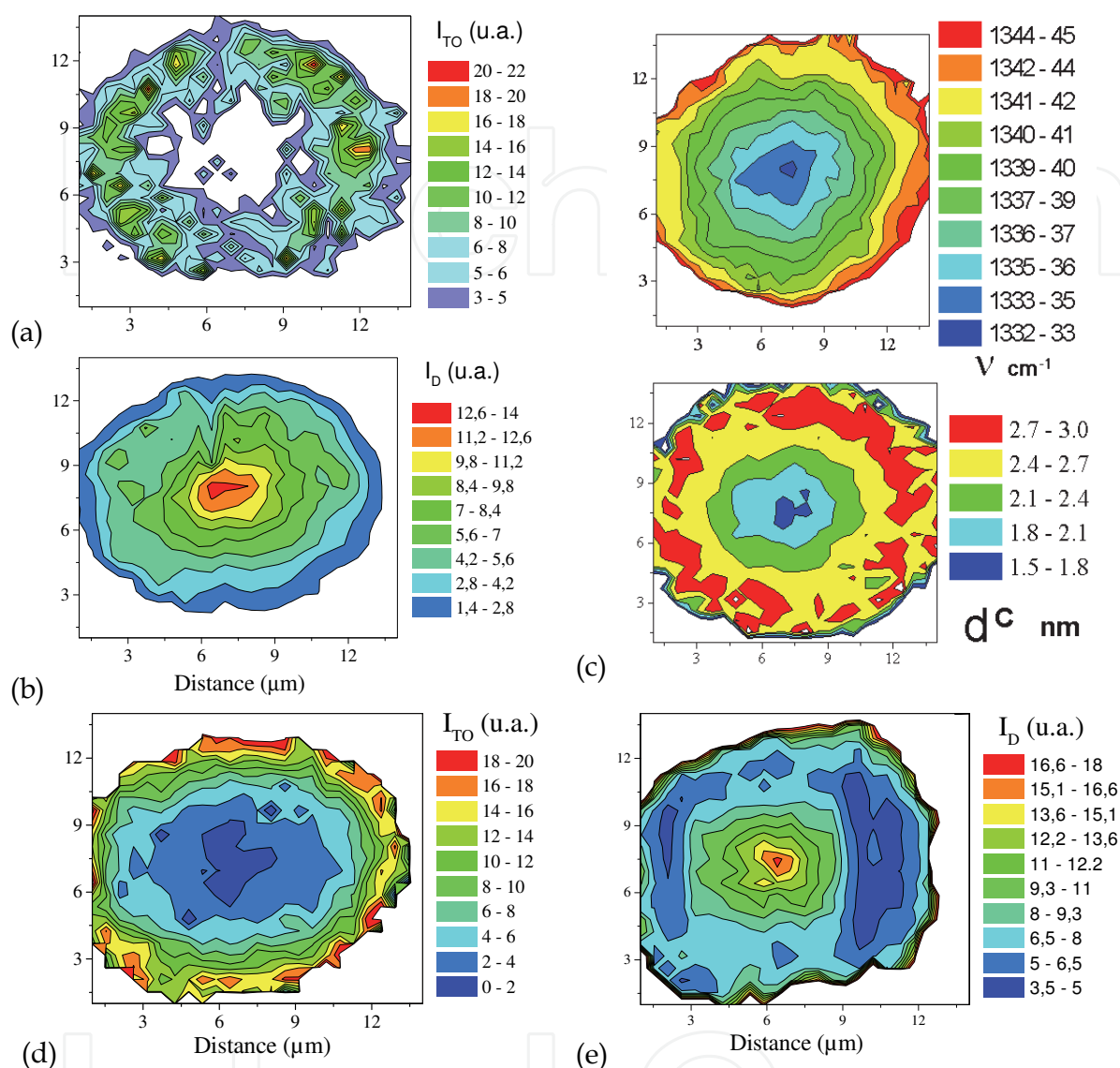


Fig. 11. Raman maps of the TO SiC (a) and D C stretching mode intensity (b) and D wavenumber (c-top) recorded on the section of a SA3™ fibre (30x30 spectra, 0.5µm step, x100 objective, λ = 632 nm). The c-bottom image is a calculation, see text. Evolution of the TO and D band intensity after a thermal treatment at 1600°C is shown in d) and e).

Because of their interesting thermal and mechanical properties, SiC composites (SiC fibres + SiC matrix) find numerous applications in the aerospace industry and new ones are expected in fusion ITER plant (Roubin et al., 2005). However, their expensive cost has to be balanced with a long lifetime, which is not yet achieved. To increase their lifetime, we first have to understand their behaviour under chemical and mechanical stresses, and thus, to characterize their nanostructure. In this section, we focus on the SiC fibres, which are analysed across their section. Indeed, this approach allows observing the chemical variations that may exist between the fibre's core and surface. Fig. 11 shows Raman maps

of the Tyranno SA3™ (Ube Industry) fibre polished sections: a full spectrum is recorded each 0.5 μm (the hyperspectrum) and after computation, Raman parameters are extracted and mapped. Figures 11a & b consider the intensity variation of the TO SiC and D carbon peaks (see also Fig. 4); this later line is assigned to the vibrations of peculiar carbon moieties, which are thought to be located at the edges of the sp<sup>2</sup> carbon grains (Fig. 10a). Fig. 11c (top) shows the wavenumber shift of the later D band. In this particular case, the wavenumber shift represents the aromaticity of the carbon species. It has been reported that this parameter also depends on the residual strain as is shown in equation 5 (Gouadec & Colombari, 2001).

$$\Delta\bar{\nu}_D = 10 \text{ cm}^{-1} / \text{GPa} \quad (5)$$

The radial anisotropy results from the fibre preparation process: the fibre is heated from outside and the departure of the H and C excess takes place at the fibre surface. Consequently, because of the thermodynamic rules, the temperature of the fibre surface is higher than that of the core, that keep C and H excess. After thermal treatment at 1600°C a better homogeneity is achieved. Obviously, the specific microstructures of the different fibre grades can be analysed using a “simpler” and faster diameter line-scan (Fig. 4).

The first maps (Figs 10a, b & c-top), representing the distribution of a simple Raman parameter, may be of limited physical interest. However, it can be translated (through models) to a property' map (Colombari, 2003). The resulting image as exemplified in (Fig. 11c-bottom) gives the distribution of physical parameters; we call it a “Smart image”.

For instance, the size of short-range ordered vibrational units in carbon moieties can be deduced from the Raman parameters. It is based on the ratio of the intensity, *I*, of the two main carbon Raman peaks (*I<sub>D</sub>*/*I<sub>G</sub>*), as first proposed by Tuinstra & Koenig, 1970.

$$I_D / I_G = C_1 / S_g \quad (6)$$

with the grain size *S<sub>g</sub>* in nm and the constant *C* = 44 for 5145.5 nm laser excitation; this formula works well for relatively large grains (>2 nm). A new model (7) takes into account the Raman efficiency, *d*, of the D<sup>1340</sup> with respect to that of G<sup>1600</sup>, as well as *R*, the ratio of atoms on the surface of each grain with respect to the bulk, *e<sub>t</sub>* the surface thickness and *L<sub>g</sub>*, the coherent length (~ the grain size of Tuinstra and Koenig model). Assuming a spherical shape of all grains the following equation can be proposed (Colombari et al., 2001).

$$d \times R \approx d \times \left[ \left( 1 - \frac{2 \times e_t}{L_g} \right)^{-3} - 1 \right] \quad (7)$$

This model has been used to calculate the carbon grains size distribution in SA3™ fibre's cross sections. We observe that the intensity ratio is much higher in the core than near the surface and the carbon grain size appears approximately 2-3 times smaller on the fibre's core than on its periphery because the thermal gradient during the process.

The Raman data can be translated through equation 5 to a map of the maximum tolerable strain (Colombari, 2003). The resulting image (Fig. 12) clearly evidences that the fibre's mechanical properties are better (~ 3.5 GPa) in the core than near the surface (~ 2 GPa).

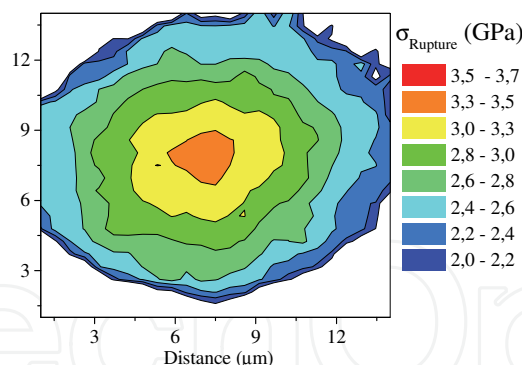


Fig. 11. Raman map of calculated ultimate tensile strength of the SiC zones in a SA3™ fibre section.

“Smart Raman images” in this section bring a lot of interesting information. First, there is a huge difference between the fibre’s core and surface with a radial gradient of physical properties as function of the fibre’ producer and additional treatments. Second, the maximum tolerable strain is observed in the fibre’s core, where the carbon species are the smallest ( $\sim 1.5$  nm). The core/skin differences are due to the elaboration process (spinning, sintering steps, etc.).

## 9. Acknowledgments

The author thanks Drs Havel, Karlin, Gouadec, Mazerolles and Parlier for their very valuable contributions to the study of SiC materials.

## 10. References

- Agrosi, G., Tempesta, G., Capitani, G.C., Scandale, E. & Siche, D. (2009). Multi-analytical study of syntactic coalescence of polytypes in a 6H-SiC sample, *J. Crystal Growth*, 311, 4784-4790.
- Alvarez-Garcia, J., Barcones, B., Perez-Rodriguez, A., Romano-Rodriguez, A., Morante, J.R., Janotti, A., Wei, S.-H. & Scheer, R., (2005). Vibrational and crystalline properties of polymorphic  $\text{CuInC}_2$  (C= Se,S), *Phys. Rev. B*, 71, 054303.
- Aoki, M., Miyazaki, M. & Nishiguchi, T. (2009). TEM Observation of the polytype transformation of Bulk SiC Ingot, in *Silicon Carbide and Related Materials 2007, Parts 1 & 2, Mater. Sci. Forum*, 600-603, 365-368.
- Baxter D., Bellosi, A. & Monteverde, F. (2000). Oxidation and burner rig corrosion of liquid phase sintered SiC, *J. Eur. Ceram. Soc.*, 20, 367-382.
- Berger, M.-H., Hochet, N. & Bunsell, A.R. (1995) Microstructure and thermomechanical stability of low-oxygen Nicalon fibers, *J. Microsc.-Oxford*, 177[3], 230-241.
- Berger, M.-H., Hochet, N. & Bunsell, A.R. (1997). Microstructure evolution of the latest generation of small-diameter SiC-based fibers tested at high temperature, *J. Microsc.-Oxford* 185 (Part 2), 243-258.
- Berger, M.-H., Hochet, N. & Bunsell A.R. (1999). Properties and microstructure of small-diameter SiC-based fibers ch. 6, pp 231-290 in *Fine Ceramic Fibers*, Ed. A.R. Bunsell & M.-H. Berger, Marcel-Dekker Inc., New-York.
- Bhargava, S., Bist, H.D. & Sahli, S., (1995). Diamond polytypes in the chemical vapor deposited diamond films, *Appl. Phys. Lett.*, 67, 1706-1708.

- Biswas, K., Rixecker, G., Wiedmann, I., Schweizer, M., Upadhyayaya, G.S. & Aldinger, F. (2001). Liquid phase sintering and microstructure-property relationships of silicon carbide ceramics with oxynitride additives, *Mater. Chem. Phys.*, 67, 180-191.
- Bodet, R., Bourrat, X., Lamon, J. & Naslain R. (1995). Tensile creep-behaviour of a silicon carbide-based fiber with low-oxygen content, *J. Mater. Sci.*, 30[3], 661-677.
- Bouillon, E., Langlais, F., Pailler, R., Naslain, R., Cruège, F., Huong, P.V., Sarthou, J.C., Delpech, A., Laffon, C., Lagarde, P. Monthieux, M. & Oberlin, A. (1991a). Conversion mechanisms of a polycarbosilane precursor into an SiC-based ceramic material, *J. Mater. Sci.*, 26, 1333-1345.
- Bouillon, E., Mocaer, D., Villeneuve, J.F., Pailler, R., Naslain, R., Monthieux, M. Oberlin, A., Guimon, C. & Pfister G. (1991b). Composition microstructure property relationships in ceramic monofilaments resulting from the pyrolysis of a polycarbosilane precursor at 800 to 1400°C, *J. Mater. Sci.*, 26, 1517-1530.
- Bunsell, A.R. & Piant, A., (2006). A review of the development of three generations of small diameter silicon carbide fibers, *J. Mater. Sci.*, 41, 823-839.
- Burns, G.T., Taylor, R.B., Xu, Y.R., Zangvil, A. & Zank G.A. (1992). High-temperature chemistry of the conversion of siloxanes to silicon carbides, *Chem. Mater.*, 4[6], 1313-1323.
- Chauvet, O., Stoto, T. & Zupirolli, L. (1992a). Hopping conduction in a nanometer-crystalline system- a SiC fibre, *Phys. Rev. B* 46[13], 8139-8146.
- Chauvet, O., Zupirolli, L. & Solomon L. (1992b). Electronic properties of disordered SiC materials, *Mater. Sci. Engr. B.-Solid State Mater. Adv. Techn.* 11[1-4], 303-306.
- Chen, J., Lien, S.C., Shin, Y.C., Feng Z.C., Kuan, C.H., Zhao, J.H. & Lu, W.J., (2009). Occurrence of polytype transformation during nitrogen doping of SiC bulk wafer, in *Silicon Carbide and Related Materials 2007, Parts 1 & 2*, *Mater. Sci. Forum*, 600-603, 39-42.
- Chi, T.T.K., Gouadec, G., Colomban, Ph., Wang, G., Mazerolles, L., Thanh, D.X. & Liem, N.Q. (2011). Off Resonance Raman Spectroscopy of Wurtzite CdS Ground to the nanoscale: Discrimination between structural and size-related effects, *J. Raman Spectrosc.*, 42, 1007-1015. doi:10.1002/jrs.2793.
- Chollon, G., Czerniak, M., Pailler, R., Bourrat, X., Naslain, R., Pillot, J.P. & Cannet, R. (1997). A model SiC-based fibre with low oxygen content prepared from polysilane precursor, *J. Mater. Sci.*, 32[4], 893-911.
- Choyke, W.J. & Pensl, G. (1997), Physical properties of SiC, *MRS Bull.*, 22[3], 25-29.
- Chung, G.-S. & Han, K.-B. (2008). H<sub>2</sub> carrier gas dependence of Young's modulus and hardness of chemical vapour deposited polycrystalline 3C-SiC thin films, *Microelectr. J.*, 39, 1413-14515.
- Colomban, Ph. (1989). Gel Technology in Ceramics, Glass-Ceramics and Ceramic-Ceramic Composites, *Ceramics Inter.*, 15, 23-50.
- Colomban, Ph., (1997). The corrosion of ceramic-matrix composites, *Mater. Sci. Forum*, 251-254, 833-844.
- Colomban, Ph., (2002). Analysis of Stress and Strain in Ceramic, Polymer and Metal Matrix Composites by Raman Spectroscopy, *Adv. Engr. Mater.* 4[8], 535-542.
- Colomban, Ph., Gouadec, G., & Mazerolles, L. (2001). Alkaline corrosion of SiC and Carbon Fibers surface. A Raman and electron microscopy study, *Proc. 103th Ann. Amer. Cer. Soc. Conf. Engr.*, *Ceramic. Trans.* 128, 157-168.
- Colomban, Ph., Gouadec, G. & Mazerolles, L. (2002). Raman analysis of materials corrosion: the example of SiC fibers, *Mater. Corr.*, 53, 306-315.

- Colomban, Ph. & Havel, M. (2002). Raman Imaging of Stress-induced Phase Transformation in Transparent ZnSe Ceramics and Sapphire Single Crystal, *J. Raman Spectrosc.*, 33[10], 789-795.
- Colomban, Ph. (2003). Raman analyses and "smart" imaging of nanophases and nanosized materials, *Spectroscopy Europe*, 15[6], 8-15.
- Colomban Ph. & Wey, M. (1997). Sol-gel control of the matrix net-shape sintering in 3D reinforced ceramic matrix composites, *J. Eur. Ceramic Soc.*, 17 [12], 1475-1483.
- Colomban, Ph. (2005). Nano/micro-structure and Property Control of Single and Multiphase Materials, ch 12, 303-339, in *Chemical Processing of Ceramics, Second Edition*, Komarneni S. & Lee B. Eds, CRC Press, Boca Raton, FL, USA.
- Corriu, R. & Lanneau, L. (1970). Application des propriétés réductrices des organomagnésiens à la preparation de nouveaux organosilanes asymétriques, *Tetrahedron Lett.*, 2, 165-168.
- Delplancke, M.P., Powers, J.M., Vandentop, G.J. & Somorjai, G.A. (1991). Preparation of  $\text{Si}_x\text{C}_y\text{H}_z$  films from methylsilane by plasma enhanced chemical vapor deposition, *Thin Solid Films*, 202[2], 289-298.
- Devaty, R.P. & Choyke, W.J., (1997). Optical characterization of silicon carbide polytypes, *phys. Stat. Sol. (a)-Appl. Res.*, 162, 5-38.
- Dkaki, M., Calcagno, L., Makthari, A.M. & Raineri V. (2001). Infrared spectroscopy and transmission electronic microscopy of polycrystalline silicon carbide, *Mater. Sci. Semicond. Process.*, 4[1-3], 201-204.
- Dirras, G.F., Djemia, P., Roussigné & Y., Jackson, K.M. (2004). Investigating the elastic properties of  $\beta$ -SiC films, *Mater. Sci. Enegn. A*, 387-389, 302-306.
- Durham, S.J.P., Shanker, K. & Drew, R.A.L. (1991). Carbothermal synthesis of silicon-nitride. Effect of reaction conditions, *J. Am. Ceram. Soc.*, 74, 31-37.
- Fayette, L., Mermoux, M., Marcus, B., Brunet, F., Germi, P., Pernet, M., Abello, L., Lucazeau, G. & Garden, J. (1995). Analysis of the fine structure of the Raman line and of X-ray reflection profiles for textured CVD diamond films, *Diamond & Related Mater.*, 4[11], 1243-1250.
- Feldman, D.W., Parker, J.H., Choyke, W.J. & Patrick, L. (1968). Phonon dispersion curves by Raman scattering in SiC polytypes 3C, 4H, 6H, 15R and 21R, *Phys. Rev.*, 173[3], 787-797
- Fritz, G., Grobe, J. & Kummer, D. (1965). Carbosilanes, *Adv. Inorg. Chem.*, 7, 349-418.
- Gouadec, G. & Colomban, Ph. (2001). Non-destructive mechanical characterization of SiC fibers by Raman spectroscopy, *J. Eur. Ceram. Soc.*, 21, 1249-1259.
- Gouadec, G., Karlin, S. & Colomban, Ph. (1998). Raman extensometry study of NLM202 and Hi-Nicalon<sup>®</sup> SiC fibres, *Composites Part B*, 29[3], 251-261.
- Gouadec, G., Colomban, Ph. & Bansal, N.P. (2001). Raman study of Hi-Nicalon-fiber-reinforced celsian composites: I, distribution and nanostructure of different phases, *J. Am. Ceram. Soc.*, 84, 1129-1135.
- Gouadec, G. & Colomban, Ph. (2007). Raman study of Nanomaterials : How spectra related to disorder, particle size and mechanical properties, *Progr. Cryst. Growth & Charact. Mater.*, 53[1], 1-56.
- Gouadec, G., Bellot-Gurlet, L., Baron, D. & Colomban, Ph. (2011). Raman mapping for the investigation of nanophased materials, ch. 4 in *Raman Imaging*, Zoubir A. Ed., Springer, in press.
- Gough, J.R.C. & Kern, D. (1967). Studies on the coating of fuel particles for the "dragon" reactor experiment, *J. Nuclear Energy*, 21[8], 623-624.

- Greil, P. (1995). Active-Filled-Controlled Pyrolysis of Preceramic Precursors, *J. Am. Ceram. Soc.*, 78[4], 835-848.
- Greil, P. (2000). Polymer derived engineering ceramics, *Adv. Engrn. Mater.* 2[6], 339-348.
- Hasegawa, Y., Feng, C.X., Song, Y.C., Song, Y.C. & Tan, Z.L. (1991). Ceramic fibers from polymer precursors containing Si-O-Ti bonds - 2 Synthesis of various types of ceramic fibers, *J. Mater. Sci.*, 26[13], 3657-3664.
- Havel, M. (2004) *Imageries Raman et Rayleigh de nanophases. Nouveaux outils pour l'étude de la corrosion de matériaux hétérogènes. Application aux fibres et composites céramiques*, Thesis, Université Paris 6, Paris.  
<http://www.ladir.cnrs.fr/pages/theses/TheseHavel.pdf>
- Havel, M. & Colomban, Ph. (2003). Skin/bulk nanostructure and corrosion of SiC based fibres. A surface Rayleigh and Raman study, *J. Raman Spectrosc.*, 34[10], 786-794.
- Havel, M. & Colomban, Ph. (2004). Rayleigh and Raman images of the bulk/surface nanostructure of SiC based fibres, *Composites Part B*, 35, 139-147.
- Havel, M. & Colomban, Ph. (2005). Raman and Rayleigh mapping of corrosion and mechanical aging in SiC fibres, *Comp. Sci. Techn.*, 65, 353-358.
- Havel, M. & Colomban, Ph. (2006). Smart Raman and Rayleigh Spectroscopy for the Analysis of Nanomaterials, *Microscopy and Analysis*, 20[3], 11-14.
- Havel, M., Baron, D. & Colomban, Ph. (2004). "Smart" Raman/Rayleigh imaging of nanosized SiC materials using the spatial correlation model, *J. Mater. Sci.*, 39, 6183-6190.
- Havel, M., Baron, D., Mazerolles, L. & Colomban, Ph. (2007). Phonon Confinement in SiC Nanocrystals: Comparison of the Size Determination using Transmission Electron Microscopy and Raman Spectroscopy, *Appl. Spectrosc.*, 61, 855-859.
- Hundhausen, M., Püsche, R., Röhr, J. & Ley, L. (2008). Characterization of defects in silicon carbide by Raman Spectroscopy, *phys. stat. sol. (b)*, 245, 1356-1368.
- Hurwitz, F.I., Farmer, S.C., Terepka, F.M. & Leonhardt T.A. (1991). Silsesquioxane-derived ceramic fibers, *J. Mater. Sci.*, 26[5], 1247-1252.
- Hurwitz, F.I., Heimann, P., Farmer, S.C. & Hembree, D.M. (1993). Characterization of the pyrolytic conversion of Polysilsesquioxanes to Silicon Oxycarbides, *J. Mater. Sci.*, 28[24], 6622-6630.
- Ischikawa, T. (1995). Recent development of the SiC fiber Nicalon and its composites including properties of the SiC fiber Hi-Nicalon for ultra high temperature, *Comp. Sci. & Techn.* 51[2], 135-144.
- Ischikawa, T., Kohtoku, Y., Kumagawa, K., Yamamura, T. & Nagasawa, T. (1998). High-strength alkali-resistant sintered SiC fibre stable to 2000°C, *Nature*, 391[6669], 773-775.
- Ischikawa, T., Yamamura, T. & Okamura, K. (1991). The oxidation resistance of Si-Ti-Co fiber produced from cross-linked organometallic polymer, *Nippon Kagaku Kaishi*, 10, 1278-1283.
- Kiflawi, I., Mardix, S. & Kalman, Z.H. (1969). Zinc sulphide needles containing new polytypes, *Acta Crystallogr. Sect. B -Structural Crystallogr. & Cryst. Chem. B*, 25 2413.
- Karlin, S. & Colomban, Ph. (1997). Raman study of the chemical and thermal degradation of as received and sol-gel embedded Nicalon and Hi-Nicalon SiC fibres used in ceramic matrix composites, *J. Raman Spectrosc.*, 28, 219-228
- Karlin, S. & Colomban, Ph. (1998). Micro Raman study of SiC fibre-oxide matrix reaction, *Composites Part B*, 29B, 41-50.

- Komatsu, S., Kobayashi, K., Sato, Y., Hirano, D., Nakamura, T., Nagata, T., Chikyo, T., Watanabe, T., Takizawa, T., Nakamura, K & Hashimoto, T. (2010). Photoinduced phase transformation in Boron Nitride: new polytypic forms of sp(3) bonded (6H- and 30H-)BN, *J. Phys. Chem. C*, 114[31], 13176-13186.
- Kosacki, I., Suzuki, T., Petrovsky, V., Anderson, H.U. & Colombari, Ph. (2002). Raman scattering and lattice defects in nanocrystalline CeO<sub>2</sub> thin films, *Solid State Ionics*, 149, 99-105
- Kosacki, I., Petrovsky, V., Anderson, H.U. & Colombari, Ph. (2002). Spectroscopy of nanocrystalline ceria and zirconia thin films, *J. Am. Ceram. Soc.*, 85[11], 2646-2650.
- Kumar, K. & Litt, M.H. (1988). A new silane polymer as a precursor to SiC, *J. Polymer Sci. Part C Polymer Lett.*, 26, 25-32.
- Kumagawa, K., Yamaoka, H., Shibuya, M. & Yamamura, T. (1998). Fabrication and mechanical properties of new improved Si-C-(O) Tyranno fiber, *Ceram. Engn. Sci. Proc.*, 19[3], 65-72.
- Langguth, K. (1995). Preparation of macro-porous SiC-Al<sub>2</sub>O<sub>3</sub> composites with polysilanes and polycarbosilanes, *Ceram. Int.*, 21, 237-242.
- Learn, A.J. & Khan, I.H. (1970). Growth morphology and crystallographic orientation of  $\beta$ -SiC films formed by chemical conversion, *Thin Solid Films*, 5, 145-155.
- Le Coustumer, P., Monthieux, M. & Oberlin, A. (1995a). Further studies of the stability of PCS-based ceramic fibers at high temperature. 1 Oxidation behaviour, *Brit. Ceram. Trans.* 94[5], 177-184 .
- Le Coustumer, P., Monthieux, M. & Oberlin, A. (1995b). Further studies of the stability of PCS-based ceramic fibers at high temperature. 2 Effect of all carbon environment, *Brit. Ceram. Trans.*, 94[5], 185-190 .
- Lee, J.-S. & Yano, T. (2004). Fabrication of short-fiber-reinforced SiC composites by polycarbosilane infiltration, *J. Eur. Ceram. Soc.*, 24, 25-31.
- Lincot, D., Mokili, B., Froment, M., Cortes, R., Bernard, M.-C., Witz, C. & Lafait, J. (1997). Phase transition and related phenomena in chemically deposited polycrystalline Cadmium Sulfide thin film, *J. Phys. Chem. B*, 101, 2174-2181.
- Lipowitz J., Rabe J.A., Ngyuen, K.T., Orr, L.D. & Androl, R.R. (1995). Structure & properties of polymer-derived stoichiometric fiber, *Ceram. Eng. Sci. Proc.*, 16[5], 55-63.
- Lipowitz J., Rabe J.A., Zangvil A. & Xu, Y. (1997). Structure & properties of SYLRAMIC™ Silicon carbide fiber - A polycrystalline, stoichiometric  $\beta$  SiC composition, *Ceram. Eng. Sci. Proc.*, 18[3], 147-157.
- Lucke, J., Hacker, J., Suttor, D. & Ziegler, G. (1997). Synthesis and characterization of silazane-based polymers as precursors for ceramic matrix composites, *Appl. Organometallic Chem.*, 11[2], 181-194.
- Marinova, M., Zoulis, G., Robert T., Mercier, F., Mantzari, A., Galben, I., Kim-Hak, O., Lorenzzi, J., Julliaguet, S., Chaussende, D., Ferro, G., Camassel, J. & Polychroniadis, E.K. (2009). Defect-induced polytype transformations in LPE grown SiC epilayers on (111) 3C-SiC seeds grown by VLS on 6H-SiC, *Physica B-Condensed Matter.*, 404[23-24], 4727-4730.
- Martin, H.P., Muller, E., Irmer, G. & Babonneau, F. (1997). Crystallisation behaviour and polytype transformation of polymer-derived silicon carbide, *J. Eur. Ceram. Soc.*, 17[5], 659-666
- MacDiarmid, A.G. (1961). Silanes and their derivatives, *Adv. Inorg. Chem.* 3, 207-256.
- Mirguet, C., Roucau, C. & Sciau, P. (2009). Transmission electron microscopy a powerful means to investigate the glazed coating of ancient ceramics, *J. Nano Research*, 8, 141-146.

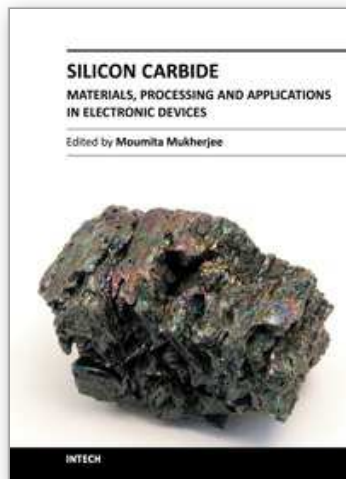


- Monthieux, M., Oberlin, A. & Bouillon, E. (1990). Relationship between microtexture and electrical properties during heat treatment of SiC fiber precursor, *Composite Sci. & Techn.*, 37, 21-35.
- Monthieux, M., Cojean, M., Delverdier, O., Le Coustumer P. & Madigou, V. (1991). Characterization of ceramic composites and of their constituents - Precursors, Fibers and Interphases, *Microsc. Microanalysis Microstructures*, 2[1], 47-57.
- Moret, R. & Huber, M. (1976). Structure of new polytypes of Titanium Sulfide. *Acta Crystallogr. Section B-Structure Sci.*, 32, 1302-1303.
- Mouchon, E. & Colombari, Ph. (1996). Microwave absorbent: preparation, mechanical properties and r.f.-microwave conductivity of SiC (and/or mullite) fibre reinforced Nasicon matrix composites, *J. Mater. Sci.*, 31, 324-334.
- Mouchon, E. & Colombari, Ph. (1995). Oxide ceramic matrix-oxide fibers woven fabric composites exhibiting dissipative fracture behavior, *Composites* 26, 175-182
- Nakashima, S., Nakakura, Y. & Inoue, Z. (1987). Structural identification of SiC polytypes by Raman scattering: 27R and 33R polytypes, *J. Phys. Soc. Jpn*, 56[1], 359-364.
- Nakashima, S. & Hangyo, M. (1991). Raman intensity profiles and the stacking structure in SiC polytypes, *Solid. State Comm.*, 80, 21-24.
- Nakashima, S. & Harima, H. (1997). Raman investigation of SiC polytypes, *phys. stat. sol. (a) Appl. Res.*, 162, 39-64.
- Nakashima, S., Katahama, H., Nakakura, Y. & Mitsuishi, A. (1986). Relative Raman intensities of the folded modes in SiC polytypes, *Phys. Rev. B*, 33[8], 5721-5729.
- Nakashima, S., Wada, A. & Inoue, Z. (1987). Raman scattering from anisotropic phonon modes in SiC polytypes, *J. Phys. Soc. Jpn*, 56, 3375-3380.
- Nakashima, S., Nakatake, Y., Harima, H., Katsuno, M. & Ohtani, N. (2000). Detection of stacking fault in 6H-SiC by Raman scattering, *Appl. Phys. Lett.*, 77[22], 3612-3614.
- Narisawa, M., Okabe, Y., Okamura, K., Taki, T. & Kamiyama, T. (2000). Silicon-29 solid state MAS NMR investigation of silicon carbide powder prepared with a precursor method, *J. Ceram. Soc. Jpn*, 108[12], 1110-1114.
- Naslain, R. (2004). Design, preparation and properties of non-oxide CMCs for application in engines and nuclear reactors: an overview, *Comp. Sci. Techn. Engrn.* 64[2], 155-170.
- Naslain, R.R., Pailler, R., Bourrat, X., Bertrand, S., Heurtevent, F., Dupel, P. & Lamouroux, F. (2001). Synthesis of highly tailored Ceramic matrix Composites by pressure pulsed CVI, *Solid State Ionics*, 141, 541-548.
- Nemanich, R.J., Solin, S.A. & Martin, R.M. (1981). Light-scattering study of boron-nitride microcrystals, *Phys. Rev. B* 23[12], 6348-6356.
- Okamura, K., Matsuzawa, T. & Hasegawa, Y. (1985). Gamma-ray irradiation curing on polycarbosilane fibers as the precursor of SiC fibers, *J. Mater. Sci.*, 4, 55-57.
- Okimura, H., Sakuma, E., Lee, J.H., Mulkaida, H., Misawa, S., Endo, K. & Yoshida, S. (1987). Raman scattering of SiC: application to the identification of heteroepitaxy of SiC polytypes, *J. Appl. Phys.* 61[3], 1134-1136.
- Ono, K. & Kurachi, Y. (1991). Kinetic Studies on beta SiC formation from homogeneous precursors, *J. Mater. Sci.*, 26, 388-392.
- Parayanthal, P. & Pollak, F.H. (1984). Raman scattering in alloy semiconductors - Spatial correlation model, *Phys. Rev. Lett.* 52[20], 1822-1825.
- Parlier, M. & Colombari, Ph. (1996). Composites à matrice céramique pour applications thermostructurales, *La Recherche Aérospatiale*, 5/6, 457-469.
- Popovska, N., Emig, G., Edie, D.D. & Rhee, B.S. (1997). Chemical vapor deposition of silicon carbide on carbon fibers with round and nonround cross-section, *High Temp. & Mater. Sci.*, 37[1], 1-11.

- Porte, L. & Sartre, A. (1989). Evidence for a silicon oxycarbide phase in the Nicalon silicon carbide fibre, *J. Mater. Sci.*, 24, 271-275.
- Richter, H, Wang, Z.P. & Ley, L. (1981). The one-phonon Raman spectrum in microcrystalline silicon, *Solid State Comm.*, 39(5), 625-629.
- Rohmfeld, S., Hundhausen, M. & Ley, L. (1998). Raman scattering in polycrystalline 3C-SiC: Influence of stacking faults, *Phys. Rev. B*, 58, 9858-9862.
- Roubin, P., Martin, C., Arnas, C., Laffon, C., Parent, P., Colomban, Ph., Pegourié, B. & Brosset, C. (2005). Raman spectroscopy and X-ray diffraction studies of some deposited carbon layers in Tore Supra, *J. Nuclear Mater.*, 337-339, 990-994.
- Ruggles-Wrenn, M.B. & Whiting, B.A. (2011). Cyclic creep and recovery behaviour of Nextel™ 720 alumina ceramic composite at 1200°C, *Mater. Sci. Eng. A*, 528[3], 1848-1856.
- Ruggles-Wrenn, M.B. & Kutsal, T. (2010). Effect of steam environment on the creep behaviour of Nextel™ 720 idem alumina-mullite ceramic composite at elevated temperature, *Composite Part A- Appl. Sci. & Manuf.*, 41[12], 1807-1816.
- Rynders, S.W., Scheeline, A. & Bohn, P.W. (1991). Structure evolution in a SiC-H film prepared from tetramethylsilane, *J. Appl. Phys.*, 69, 2951-2960.
- Sacks, M.D. (1998). Effect of composition and heat treatment conditions on the tensile strength and creep resistance of SiC-based fibers, *J. Eur. Ceram. Soc.*, 19[13-14], 2305-2315.
- Salvador, G. & Sherman, W.F. (1991), Pressure dependence of the Raman spectrum in 6H-silicon carbide, *J. Mol. Struct.*, 247, 373-384.
- Sasaki, Y. Nishina, Y., Sato, M. & Okamura, K. (1987). Raman study of SiC fibers made from PCS, *J. Mater. Sci.*, 22, 443-448.
- Schmidt, W.R., Interrante, L.V., Doremus, R.H., Trout, T.K., Marchetti, P.S. & Maciel, G.E. (1991). Pyrolysis Chemistry of an Organometallic precursor to Silicon Carbide, *Chem. Mater.*, 3, 257-267.
- Schneide, J. & Kirby, R.D. (1972). Raman scattering of ZnS polytypes, *Phys. Rev. B*, 6[4], 1290-1296.
- Sciau, Ph., Salles, Ph., Roucau, C., Mehta, A. & Benassayag, G. (2009). Applications of focused ion beam for preparation of specimens of ancient ceramics for electron microscopy and Synchrotron X-ray studies, *Micron*, 40[5-6], 597-604.
- Sha, J.J., Nozawa, T., Park, J.S., Katoh, Y. & Kohyama, A. (2004). Effect of heat treatment on the tensile strength and creep resistance of advanced SiC fibers, *J. Nuclear Mater.*, 329-333, 592-596.
- Simon, G. & Bunsell, A.R. (1984). Mechanical and structural characterization of the Nicalon silicon-carbide fiber, *J. Mater. Sci.*, 19[11], 3649-3657.
- Song, Y. Feng, C. Tan, Z. & Lu, Y. (1990). Structure and properties of polytitanocarbo-silane as the precursor of SiC-TiC fiber, *J. Mater. Sci. Lett.*, 9[11], 1237-1243.
- Stewart, R.M., Dando, N.R., Seyferth, D. & Perrota, A.J., (1991). Characterization of Hydridomethyl-polysilazane - A precursor to SiC/SiN ceramics, *Abtr. Paper Am. Chem. Soc.*, 202, 340-POLY.
- Tanaka, H. & Kurachi, Y. (1988). Synthesis of beta-SiC powder from organic precursor and its sinterability, *Ceram. Int.*, 14, 109-115.
- Tanaka, A., Onari, S. & Arai, T. (1993). Low-frequency Raman scattering from CdS microcrystals embedded in a germanium dioxide glass matrix, *Phys. Rev. B* 47[3], 1237-1243.

- Tanaka, T., Tamari, N., Kondoh, I. & Iwasa, M. (1995). Fabrication and evaluation of 3-dimensional Tyranno fiber-reinforced SiC composites by repeated infiltration of polycarbosilane, *J. Ceram. Soc. Jpn*, 103, 1-5.
- Tanaka, T., Tamari, N., Kondoh, I. & Iwasa, M., (1996). Fabrication and mechanical properties of 3-dimensional Tyranno fiber reinforced SiC composites by repeated infiltration of polycarbosilane, *J. Ceram. Soc. Jpn*, 104, 454-457.
- Tuinstra, F.T., Koenig, J.I. (1970). Raman spectrum of Graphite, *J. Chem. Phys.*, 53, 1126-1130.
- Tomita, T., Saito, S., Baba, M., Hundhausen, M., Suemoto, T. & Nakashima, S. (2000). Selective resonance effect of the folded longitudinal phonon modes in the Raman spectra of SiC, *Phys. Rev. B*, 62, 12896-12901.
- Toreki, W., Batich, C.D. & Choi, G.J. (1991). High molecular weight polycarbosilane as a precursor to oxygen free SiC fibers, *Abstr. Paper Am. Chem. Soc.*, 202, 360-POLY
- Toreki, W.M., Batich, C.D., Sacks, M.D., Saleem, M., Choi, G.J. & Morrone, A.A. (1992). Polymer-derived silicon-carbide fibres with low-oxygen content and improved thermomechanical stability, *Comp. Sci. Techn. Eng.*, 1351[2], 145-159.
- Tronc, E., Moret, R. & Legendre, J.J. & Huber, M. (1975). Refinement of polytypes structure 12R Ti<sub>8</sub>S<sub>12</sub>. *Acta Crystallogr. Section B-Structure Sci.*, 31, 2800-2804.
- Yajima, S., Okamura, K., Tanaka, J. & Hayase, T. (1980). Synthesis of aluminium composite reinforced with continuous SiC Fiber obtained from the precursor fiber of an organo-silicon precursor polymer, *J. Mater. Sci.*, 15, 2130-2131.
- Yang, Y.M., Liu, X.W., Tan, Z.L., Yang, S.J., Lu, Y. & Feng, C.X. (1991). Synthesis of SiC fiber with low oxygen content and high tensile strength using a polyblend precursor, *J. Mater. Sci.*, 26[19], 5167-5170.
- Yano, M., Utatsu, T., Iwai, Y. & Inoue, F. (1995). A Raman scattering study on the interface sharpness of INAS/ALSB/GASB/ALSB polytypes superlattices grown by molecular-beam epitaxy. *J. Cryst. Growth*, 150 [1-4], 868-873.
- Weber, W.H., Hass, K.C. & McBride, J.R. (1993). Raman study of CeO<sub>2</sub> - 2<sup>nd</sup> order scattering, lattice dynamics and particle size effects, *Phys. Rev. B*, 48[1], 178-185.
- Wu, Y.-C., Wang, S.-F. & Lu, H.-Y. (2006). Stacking Faults and Stacking Fault Energy of Hexagonal Barium Titanate, *J. Am. Ceram. Soc.*, 89, 3778-3787.
- Wu, Y.-C., Wang, S.-F. & Chen, S.-H. (2009). Microstructural Investigation of Ba(Ti<sub>(1-x)</sub>Mn<sub>x</sub>)O<sub>3</sub> Ceramics with 6H- and 12R-polytypes, *J. Am. Ceram. Soc.*, 92, 2099-2108.

IntechOpen



## **Silicon Carbide - Materials, Processing and Applications in Electronic Devices**

Edited by Dr. Moumita Mukherjee

ISBN 978-953-307-968-4

Hard cover, 546 pages

**Publisher** InTech

**Published online** 10, October, 2011

**Published in print edition** October, 2011

Silicon Carbide (SiC) and its polytypes, used primarily for grinding and high temperature ceramics, have been a part of human civilization for a long time. The inherent ability of SiC devices to operate with higher efficiency and lower environmental footprint than silicon-based devices at high temperatures and under high voltages pushes SiC on the verge of becoming the material of choice for high power electronics and optoelectronics. What is more important, SiC is emerging to become a template for graphene fabrication, and a material for the next generation of sub-32nm semiconductor devices. It is thus increasingly clear that SiC electronic systems will dominate the new energy and transport technologies of the 21st century. In 21 chapters of the book, special emphasis has been placed on the "materials" aspects and developments thereof. To that end, about 70% of the book addresses the theory, crystal growth, defects, surface and interface properties, characterization, and processing issues pertaining to SiC. The remaining 30% of the book covers the electronic device aspects of this material. Overall, this book will be valuable as a reference for SiC researchers for a few years to come. This book prestigiously covers our current understanding of SiC as a semiconductor material in electronics. The primary target for the book includes students, researchers, material and chemical engineers, semiconductor manufacturers and professionals who are interested in silicon carbide and its continuing progression.

### **How to reference**

In order to correctly reference this scholarly work, feel free to copy and paste the following:

Philippe Colombari (2011). SiC, from Amorphous to Nanosized Materials, the Example of SiC Fibres Issued of Polymer Precursors, Silicon Carbide - Materials, Processing and Applications in Electronic Devices, Dr. Moumita Mukherjee (Ed.), ISBN: 978-953-307-968-4, InTech, Available from:

<http://www.intechopen.com/books/silicon-carbide-materials-processing-and-applications-in-electronic-devices/sic-from-amorphous-to-nanosized-materials-the-exemple-of-sic-fibres-issued-of-polymer-precursors>

**INTECH**  
open science | open minds

### **InTech Europe**

University Campus STeP Ri  
Slavka Krautzeka 83/A  
51000 Rijeka, Croatia  
Phone: +385 (51) 770 447

### **InTech China**

Unit 405, Office Block, Hotel Equatorial Shanghai  
No.65, Yan An Road (West), Shanghai, 200040, China  
中国上海市延安西路65号上海国际贵都大饭店办公楼405单元  
Phone: +86-21-62489820

[www.intechopen.com](http://www.intechopen.com)

Fax: +385 (51) 686 166  
www.intechopen.com

Fax: +86-21-62489821

IntechOpen

IntechOpen

© 2011 The Author(s). Licensee IntechOpen. This is an open access article distributed under the terms of the [Creative Commons Attribution 3.0 License](#), which permits unrestricted use, distribution, and reproduction in any medium, provided the original work is properly cited.

IntechOpen

IntechOpen